Microbiology and Infectious Disease

A dynamic bactofilin cytoskeleton cooperates with an M23 endopeptidase to control bacterial morphogenesis

Reviewed Preprint

Revised by authors after peer review.

About eLife's process

Reviewed preprint version 2
January 11, 2024 (this version)

Reviewed preprint version 1
April 26, 2023

Posted to preprint server
March 1, 2023

Sent for peer review
February 26, 2023

Sebastian Pöhl, Manuel Osorio-Valeriano, Emöke Cserti, Jannik Harberding, Rogelio Hernández-Tamayo, Jacob Biboy, Patrick Sobetzko, Waldemar Vollmer, Peter L. Graumann, Martin Thanbichler

Department of Biology, University of Marburg, Marburg, Germany • Max Planck Institute for Terrestrial Microbiology, Marburg, Germany • Department of Chemistry, University of Marburg, Marburg, Germany • Center for Synthetic Microbiology (SYNMIKRO), Marburg, Germany • Centre for Bacterial Cell Biology, Biosciences Institute, Newcastle University, Newcastle upon Tyne, United Kingdom • Institute for Molecular Bioscience, The University of Queensland, Brisbane, Australia

Abstract

Bactofilins have emerged as a widespread family of cytoskeletal proteins with important roles in bacterial morphogenesis, but their precise mode of action is still incompletely understood. In this study, we identify the bactofilin cytoskeleton as a key regulator of cell growth in the stalked budding alphaproteobacterium *Hyphomonas neptunium*. We show that, in this species, bactofilin polymers localize dynamically to the stalk base and the bud neck, with their absence leading to unconstrained growth of the stalk and bud compartments, indicating a central role in the spatial regulation of cell wall biosynthesis. Database searches reveal that in a range of different species bactofilin genes are clustered with genes for cell wall hydrolases of the M23 peptidase family, suggesting a functional connection between these two types of proteins. In support of this notion, we find that the *H. neptunium* M23 peptidase homolog LmdC interacts directly with bactofilin *in vitro* and is required for proper cell shape *in vivo*. Complementary studies in the spiral-shaped alphaproteobacterium *Rhodospirillum rubrum* again reveal a close association of its bactofilin and LmdC homologs, which co-localize at the inner curve of the cell, modulating the degree of cell curvature. Collectively, these findings demonstrate that bactofilins and M23 peptidases form a conserved functional module that promotes local changes in the mode of cell wall biosynthesis, thereby driving cell shape determination in morphologically complex bacteria.

eLife assessment

The manuscript explores the interplay between cytoskeletal bactofilins and cell wall hydrolases in bacterial morphogenesis, utilizing a range of methodologies from bacteriological to biochemical. The study provides **important** insights into bactofilin polymers' control over peptidoglycan synthesis and the identification of LdmC, supported by a comprehensive array of genetic, bioinformatic, biochemical, and biophysical tools. These **convincing** findings propose a conserved module governing bacterial morphogenesis, emphasizing the direct association of cell wall remodeling enzymes with a dynamic cytoskeleton, akin to mechanisms observed in other cellular processes such as cell growth and division.

Introduction

Bacteria come in a variety of different cell shapes, which can be further modified by the formation of cellular extensions such as branches or stalks (Kysela et al., 2016; Yang et al., 2016). Their morphology can change as a function of the cell cycle or in response to environmental cues to ensure optimal fitness in the given ecological niche or growth conditions (van Teeseling et al., 2017; Yang et al., 2016). In the vast majority of species, cell shape is determined by the peptidoglycan cell wall, a complex macromolecule composed of glycan chains that are crosslinked by short peptides (Typas et al., 2012; Vollmer et al., 2008). The synthesis of this mesh-like structure is achieved by an array of synthetic and lytic enzymes that are typically combined into multi-protein complexes and associated with regulatory factors and cytoskeletal elements to facilitate the coordination and spatiotemporal regulation of their activities (Egan et al., 2020; Rohs and Bernhardt, 2021).

Basic spherical, rod-like and hyphal shapes are generated by the combined action of the cell division and cell elongation machinery (Margolin, 2009; Rohs and Bernhardt, 2021). In most bacteria, cell division is executed by the divisome, which is organized by the tubulin homolog FtsZ and mediates cell constriction and the synthesis of the new cell poles prior to cytokinesis (McQuillen and Xiao, 2020). Cell elongation, by contrast, can be achieved by various types of cell wall-biosynthetic complexes, including the so-called elongasome, which is organized by the actin homolog MreB and mediates the dispersed incorporation of new cell wall material along the lateral cell walls (Shi et al., 2018), or different cell pole-associated complexes that promote polar growth of the cell body (Brown et al., 2011). More complex cell shapes are generated with the help of accessory systems that either modulate the activity of the generic cell elongation machinery or have peptidoglycan biosynthetic activity on their own, thereby locally modifying the structure of the peptidoglycan layer (Taylor et al., 2019).

A particularly widespread family of cytoskeletal proteins implicated in cell shape modification are the bactofilins. They are characterized by a conserved central Bactofilin A/B domain (InterPro ID: IPR007607; Paysan-Lafosse et al., 2022) with a barrel-like β-helical fold that is typically flanked by short disordered terminal regions (Kühn et al., 2010; Shi et al., 2015; Vasa et al., 2015). Bactofilins polymerize spontaneously without the need for nucleotide cofactors (Koch et al., 2011; Kühn et al., 2010), driven by head-to-head and tail-to-tail interactions between the core domains of neighboring molecules (Deng et al., 2019). Lateral interactions between individual protofilaments can then give rise to higher-order assemblies, such as bundles or two-dimensional sheets (Kühn et al., 2010; Vasa et al., 2015; Zuckerman et al., 2015). Previous work has suggested that bactofilin polymers typically associate with the inner face of the cyto-plasmic membrane and localize to regions of high membrane curvature (Caccamo et al., 2020; Hay et al.,

1999; Kühn et al., 2010; Lin et al., 2017; Taylor et al., 2020). These structures have been co-opted as localization determinants and assembly platforms by several different morphogenetic systems.

For instance, bactofilin homologs were reported to contribute to rod-shape maintenance in *Myxococcus xanthus* (Koch et al., 2011), the establishment of helical cell shape in the human pathogen *Helicobacter pylori* (Sycuro et al., 2010; Taylor et al., 2020) as well as the modulation of cell helicity in the spiral-shaped bacterium *Leptospira biflexa* (Jackson et al., 2018). Apart from modulating general cell shape, they were found to have an important role in the formation of cellular extensions known as stalks, which are wide-spread among alphaproteobacterial species (Wagner and Brun, 2007). Stalks are elongated protrusions of the cell envelope that are filled with a thin thread of cytoplasm and grow through zonal incorporation of cell wall material at their base (Aaron et al., 2007; Randich and Brun, 2015). In *Caulobacter crescentus* and *Asticcacaulis biprosthecum*, bactofilin polymers were shown to localize to the stalk base to direct proper stalk formation. In *C. crescentus*, they recruit a cell wall synthase that contributes to stalk elongation, with their absence leading to a reduction in stalk length (Kühn et al., 2010). In *A. biprosthecum*, by contrast, bactofilin acts as a central topological regulator that is required to efficiently initiate stalk formation and limit peptidoglycan biosynthesis to the stalk base. Its absence leads to the development of pseudostalks, which are much shorter and wider than normal stalks and irregularly shaped, likely due to unrestrained peptidoglycan biosynthesis through the entire stalk envelope (Caccamo et al., 2020).

While stalks are often accessory structures with highly specialized functions (Klein et al., 2013; Persat et al., 2014; Wagner and Brun, 2007), stalked budding bacteria such as *Hyphomonas neptunium* and other members of the *Hyphomonadaceae* and *Hyphomicrobiaceae* use them as integral parts of the cell with key roles in cell growth and division (Moore, 1981). *H. neptunium* has a biphasic life cycle (Wali et al., 1980), in which a non-replicative, motile swimmer cell sheds its single polar flagellum and differentiates into a replicative, sessile stalked cell (**Figure 1—figure supplement 1**). Unlike most widely studied model species, it does not divide by binary fission but instead produces new offspring through the formation of buds at the tip of the stalk. As the terminal stalk segment gradually dilates, a flagellum is formed at the pole opposite the stalk. After DNA replication and translocation of one of the sister chromosomes through the stalk into the bud compartment (Jung et al., 2019), cytokinesis occurs at the bud neck, releasing a new swimmer cell. While the newborn cell first needs to differentiate into stalked cells to start replication, the stalked mother cell restores the stalk and then immediately re-enters the next budding cycle (Jung et al., 2019; Wali et al., 1980). The developmental program of *H. neptunium* involves several switches in the pattern of peptidoglycan biosynthesis (Cserti et al., 2017). After birth, swimmer cells increase in size by dispersed incorporation of new cell wall material throughout the cell body. Stalk formation is then achieved by zonal growth at the stalk base, followed by localized dispersed growth of the stalk-terminal bud compartment and, finally, zonal peptidoglycan synthesis at the site of cell division. The pattern of new cell wall synthesis is similar to the localization pattern of elongasome components (Cserti et al., 2017), suggesting the involvement of this machinery in all growth phases. However, the underlying regulatory mechanisms are still unknown.

In this study, we identify the bactofilin cytoskeleton as a central player in the regulation of cell growth of *H. neptunium*. We show that the lack of bactofilins causes severe morphological defects, resulting from unconstrained growth of the stalk and bud compartments. In line with this finding, bactofilin polymers localize dynamically to the stalk base and then to the incipient bud neck prior to the onset of bud formation, acting as a barrier that retains the cell wall biosynthetic machinery in the respective growth zones. Notably, in a broad range of species, bactofilin genes lie adjacent to genes encoding putative M23 peptidases. We show that the corresponding *H. neptunium* homolog, LmdC, is an essential bitopic membrane protein with peptidoglycan hydrolase activity that interacts directly with bactofilin through its N-terminal cytoplasmic tail. Its CRISPRi-mediated depletion also results in unconstrained cell growth, confirming its functional connection to

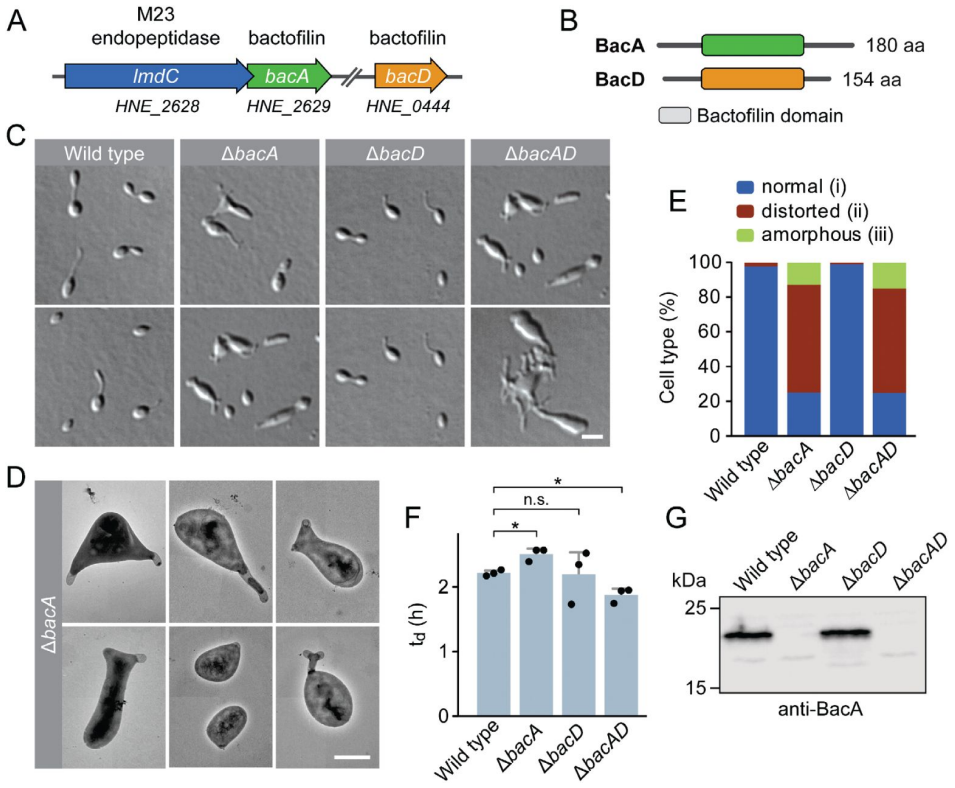

Figure 1.

Bactofilin BacA is required for proper cell morphology in *H. neptunium*.

(A) Schematic representation of the two bactofilin genes present in the *H. neptunium* genome. *bacA* lies adjacent to the M23 peptidase gene *lmdC*. Arrows indicate the direction of transcription. **(B)** Domain organization of BacA and BacD from *H. neptunium*. The bactofilin polymerization domain (colored boxes) is flanked by non-structured N- and C-terminal regions. **(C)** Morphology of *H. neptunium* bactofilin mutants. Shown are representative cells of strains LE670 (wild type), EC28 (Δ*bacA*), EC23 (Δ*bacD*) and EC33 (Δ*bacAD*), imaged by differential interference contrast (DIC) microscopy. Bar: 4 µm. **(D)** Transmission electron micrographs of Δ*bacA* cells at the early stalked-cell stage. Bar: 1 µm. **(E)** Quantification of the proportion of phenotypically abnormal stalked and budding cells in cultures of the strains analyzed in panel C (n = 100 cells per strain). **(F)** Doubling times of the indicated *H. neptunium* strains. Bars represent the mean (± SD) of three independent experiments (dots). Statistical significance was determined using Welch's non-paired t-test (*, $p<0.05$; n.s., not significant). **(G)** Immunoblot analysis of the strains shown in panel C, performed using anti-BacA antibodies.

bactofilin. The conservation of this interaction is further verified by studies of the spiral-shaped alphaproteobacterium *Rhodospirillum rubrum*. We show that the bactofilin and LmdC homologs of this species co-localize at the inner curve of the cell, forming filamentous assemblies that modulate the degree of cell curvature. Their interaction is abolished by amino acid exchanges in the cytoplasmic tail of LmdC, confirming a key role of this region in the recruitment of LmdC. Together, these results demonstrate a conserved functional interaction between bactofilins and M23 peptidases that is important for the control of cell growth in morphologically complex bacteria.

Results

The bactofilin cytoskeleton is required for cell shape determination in *H. neptunium*

The *H. neptunium* chromosome contains two open reading frames that encode bactofilin homologs, HNE_0444 and HNE_2629 (Badger et al., 2006). Reciprocal BLAST analysis using the two bactofilins described in the close relative *C. crescentus* identified HNE_2629 as a potential ortholog of *C. crescentus* BacA (43% identity, 60% similarity). By contrast, HNE_0444 was only distantly related (<30% identity) to either of the two proteins. Based on these results, we propose to designate the two bactofilin homologs of *H. neptunium* BacA (HNE_2629) and BacD (HNE_0444), respectively. *bacA* forms a putative bicistronic operon with *lmdC*, an essential gene encoding an M23 peptidase homolog (Cserti et al., 2017) (**Figure 1A**). The two genes overlap by 17 base pairs, suggesting that their expression is closely coupled. *bacD*, by contrast, is not part of an operon. Both BacA and BacD display the typical architecture of bactofilins, with a central polymerization domain flanked by short non-structured N- and C-terminal regions (**Figure 1B**).

To investigate the role of bactofilins in *H. neptunium*, we generated mutant strains in which *bacA* and *bacD* were deleted either individually or in combination and analyzed their phenotypes (**Figure 1**). The Δ*bacA* and Δ*bacAD* cells showed severe morphological defects, as reflected by irregularly shaped, elongated and/or oversized cells, buds directly fused with the mother cell body, branched stalks, and multiple wide protrusions that emerged from the cells in an apparently random fashion (**Figure 1C-E**), reminiscent of the pseudostalks reported for a bactofilin-deficient *A. biprosthecum* mutant (Caccamo et al., 2020). Surprisingly, these growth defects did not have any major defects on the doubling time (**Figure 1—figure supplement 2F**). The wild-type phenotype could be largely restored by expressing an ectopic copy of *bacA* under the control of a copper-inducible promoter, even though BacA accumulated to lower-than-normal levels under this condition, confirming the absence of polar effects (**Figure 1—figure supplement 2A-D**). The deletion of *bacD*, by contrast, did not cause any obvious cell shape defects (**Figure 1C,E,F** and **Figure 1—figure supplement 2E**). Moreover, neither *bacD* deletion nor *bacD* overexpression had any influence on the proportion of distorted or amorphous cells in the Δ*bacA* background (**Figure 1C,F** and **Figure 1— figure supplement 2C,F**). These results demonstrate that BacA has a critical role in the regulation of cell growth in *H. neptunium*, whereas BacD might be an auxiliary factor of so-far unknown function, similar to BacB in *C. crescentus* (Kühn et al., 2010).

To obtain more insight into the dynamics of cell growth in the Δ*bacA* mutant and identify the initial phenotypic defects induced upon BacA depletion, we imaged a conditional *bacA* mutant after its transfer from permissive to restrictive conditions on an agarose pad (**Figure 2A,B**). Following cells at the swimmer-to-stalked cell transition, we observed that stalk formation initially proceeded as in the wild-type strain. However, as BacA was gradually depleted, stalk elongation ceased and the stalk structure started to widen and eventually develop multiple bulges that kept on expanding in an apparently uncontrolled manner. Thus, BacA appears to be required to maintain the polar growth zone at the stalk base, with its absence leading to unconstrained

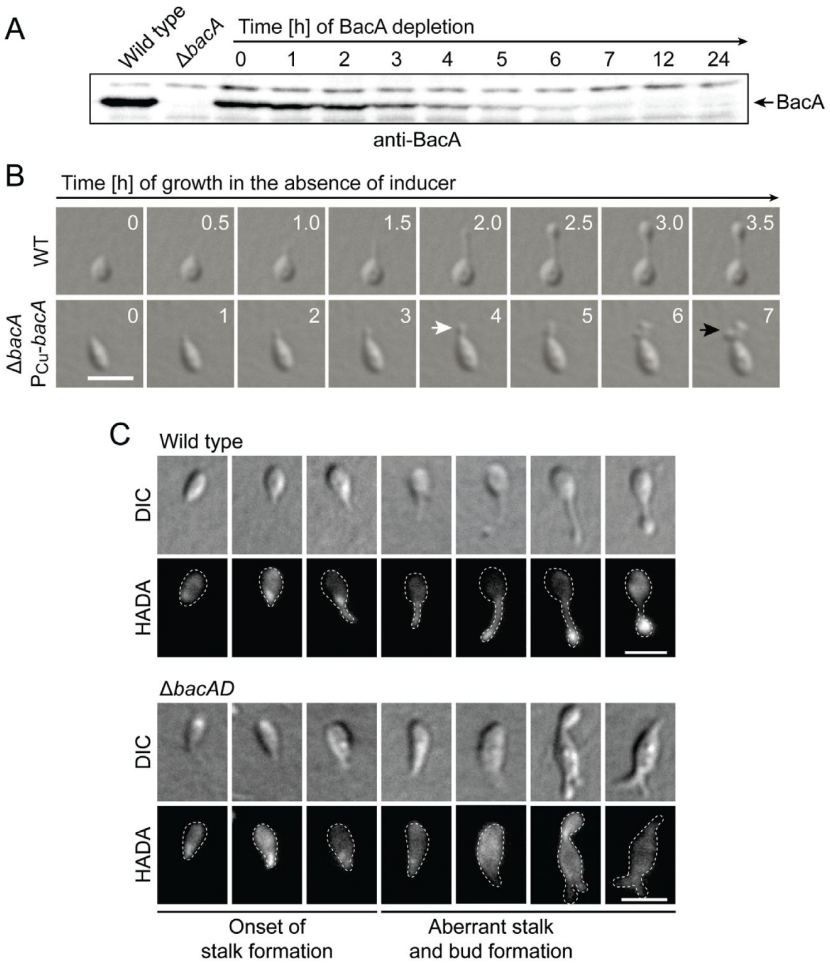

Figure 2.

Lack of BacA leads to uncontrolled growth of the stalk and bud compartments.

(A) Immunoblot showing the levels of BacA in strain EC41 (Δ*bacA* PCu-*bacA*) over the course of BacA depletion. Cells were grown in copper-containing medium, washed and transferred to inducer-free medium. At the indicated time points, samples were withdrawn and subjected to immunoblot analysis. Strains LE670 (wild type) and EC28 (Δ*bacA*) were included as controls. The position of BacA is indicated. **(B)** Morphological defects induced by BacA depletion. Cells of strains LE670 (wild type) and EC41 (Δ*bacA* PCu-*bacA*) were grown in medium containing 0.5 mM CuSO4, washed, and incubated for 6 h in inducer-free medium before they were transferred onto ASS-agarose pads lacking inducer and imaged at the indicated time points. Bar: 2 µm. **(C)** Changes in the growth pattern of *H. neptunium* in the absence of bactofilins. Cells of strains LE670 (wild type) and EC33 (Δ*bacAD*) were stained with the fluorescent D-amino acid HADA prior to analysis by fluorescence microscopy. Shown are representative images of cells at different developmental stages. Bars: 2 µm.

growth of the stalk cell wall. To follow the fate of bactofilin-deficient cells over a prolonged period of time, we monitored Δ*bacAD* cells in a flow-cell system, which ensured optimal nutrient supply throughout the course of the experiment and led to a looser packing of cells, thereby facilitating their visual analysis (**Figure 2—figure supplement 1** and **Figure 2—video 1**). In this setup, cells again started growth by the formation of irregularly shaped stalks that started to branch, with branches developing either into extensive hyphal-like structures or large, amorphous compartments that may represent morphologically aberrant buds. At irregular intervals, cells divided at the junctions between hyphal and bulged cellular segments, releasing smaller amorphous fragments and, occasionally, also cells with close-to-normal morphology. Wild-type cells, by contrast, showed the usual growth pattern when cultivated under these conditions (**Figure 2—video 1**). Together, these results underscore the importance of BacA in the spatiotemporal control of cell growth in *H. neptunium*.

To obtain more detailed information about the dynamics of cell wall biosynthesis in the absence of bactofilins, we performed pulse-labeling studies with the fluorescent D-amino acid HADA, which is rapidly incorporated into peptidoglycan when added to the culture medium, thus marking regions of ongoing cell wall biosynthesis (Kuru et al., 2015). Wild-type cells showed the typical succession of growth modes, with dispersed growth in swimmer cells, zonal growth at the stalk base in stalked cells and localized dispersed growth in the nascent bud (**Figure 2C**). In the Δ*bacAD* background, by contrast, this switch in the growth modes was abolished. Cells with close-to-normal morphology that had just initiated stalk formation still showed a distinct fluorescent focus at the stalked pole, suggesting that the initial recruitment of the machinery responsible for stalk formation occurred in a bactofilin-independent manner. However, all other cell types, including amorphous cells with aberrant stalk- and bud-like extensions, only displayed diffuse fluorescence, which points to uncontrolled growth through dispersed incorporation of new peptidoglycan throughout the entire cell envelope. These findings support the notion that the bactofilin cytoskeleton is required to limit cell wall biosynthesis to the different growth zones of *H. neptunium*.

The *H. neptunium* bactofilin homologs assemble into stable filamentous structures

Despite their severe cell shape defects, the Δ*bacA* and Δ*bacAD* mutants showed close-to-normal growth rates. Moreover, muropeptide analysis showed that the global composition of their peptidoglycan remained essentially unchanged (**Figure 2—figure supplement 2B** and **Figure 2—Dataset 1**). These findings suggested that BacA might affect cell wall composition at a local scale or act mainly by modulating the activity of the generic cell elongation machinery. To further investigate the role of bactofilins in *H. neptunium*, we first aimed to verify the ability of the proteins to assemble into polymeric scaffolds. A model of the structure of BacA generated with AlphaFold-Multimer (Evans et al., 2022) suggested that the protein adopted a β-helical fold and polymerized through head-to-head and tail-to-tail interactions among different subunits (**Figure 3A**), as revealed previously in experimental studies (Deng et al., 2019; Shi et al., 2015). Consistent with this prediction, purified BacA produced a mixture of long filaments, filament bundles and two-dimensional polymeric sheets *in vitro*, which could be readily visualized by transmission electron microscopy (**Figure 3B**). Moreover, upon heterologous co-expression in *Escherichia coli*, fluorescently tagged derivatives of BacA and BacD co-localized into extended filamentous structures that were associated with the cell envelope (**Figure 3C** and **Figure 3—figure supplement 1A**). The BacA fusion formed qualitatively similar structures when produced alone, whereas the BacD fusion condensed into tight foci in the absence of BacA (**Figure 3—figure supplement 1B,C**). These results confirm the polymeric nature of bactofilin assemblies in *H. neptunium* and suggest that BacA and BacD interact with each other *in vivo*.

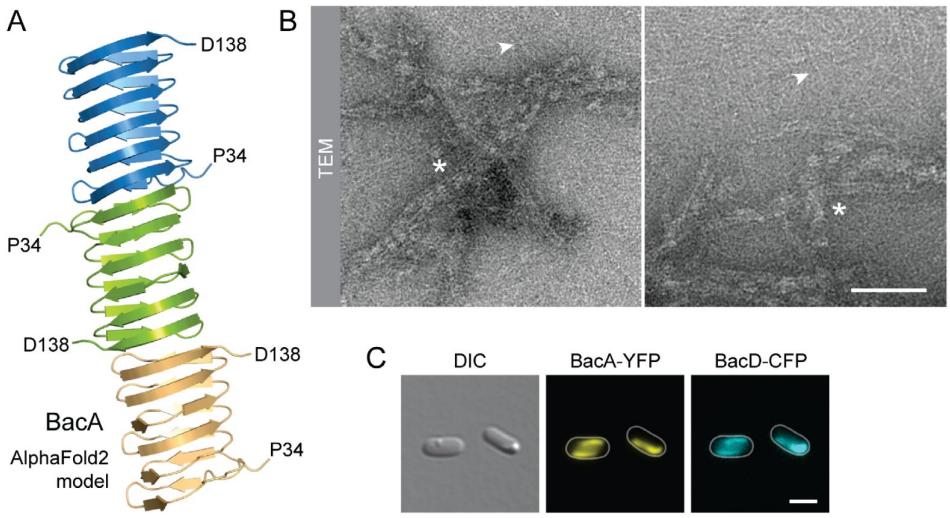

Figure 3.

BacA and BacD co-polymerize into filamentous structures.

(A) Model of a BacA trimer generated with AlphaFold-Multimer (Evans et al., 2022). Only residues P34-D138 are shown for each subunit. **(B)** Visualization of BacA polymers. Purified BacA-His6 was stained with uranyl acetate and imaged by transmission electron microscopy (TEM). Arrowheads point to BacA filaments. Asterisks indicate filament bundles and sheets. Bars: 200 nm. **(C)** Copolymerization of BacA and BacD after heterologous co-expression in *E. coli*. Cells of *E. coli* BL21(DE3) transformed with plasmid pEC121 (PT7-*bacA-eyfp* PT7-*bacD-ecfp*) were grown in LB medium containing 5 % glucose and induced with 0.5 mM IPTG prior to imaging. Bar: 3 µm.

Bactofilins localize dynamically to the boundaries of the *H. neptunium* growth zones

Next, we sought to investigate the localization dynamics of the bactofilin cytoskeleton *in vivo*. To this end, we generated strains producing fluorescently tagged BacA or BacD derivatives in place of the native proteins (**Figure 4—figure supplement 1**). Time-lapse microscopy analysis of cells producing a BacA-YFP fusion on agarose pads (**Figure 4A**) revealed that the protein was localized to the new cell pole in swimmer cells and remained associated with the stalk base during the initial phase of stalk formation. At some point, it appeared to attach to the stalk structure and then move away from the base as new cell wall material was inserted. Subsequently, stalk elongation ceased and the terminal stalk segment, delimited by the bactofilin assembly, started to swell and develop into a bud, gradually displacing BacA-YFP in the direction of the stalk base as its size increased. After cell division, both the mother cell and the newborn swimmer cells showed a fluorescent focus, indicating that the bactofilin assembly was split during cell division. To monitor the dynamics of the bactofilin cytoskeleton over multiple division cycles, we analyzed the same strain in a flow-cell system (**Figure 4—figure supplement 2** and **Figure 4—videos 1-3**). Under these conditions, the small, newborn swimmer cells were washed away immediately after cytokinesis, preventing the formation of microcolonies around the mother cell. We observed that cell division occurred at a small distance from the BacA-YFP focus, leaving a short stalk-terminal segment in between the bactofilin assembly and the stalk tip. After cytokinesis, the stalk elongated again prior to the initiation of the next budding event. Notably, BacA-YFP was only occasionally detected at the stalked pole during the stalk restoration phase, suggesting that the bactofilin cytoskeleton no longer plays a major role in stalk growth once the stalk structure has been established.

To verify the behavior observed in the time-lapse studies, we performed a population-wide analysis of the BacA-YFP localization pattern, based on snap-shot images of exponentially growing cells. A demographic analysis confirmed that the protein localizes to the new cell pole in swimmer cells, remains at the stalk base in cells with short stalks and then moves to a position close to the distal end of the stalk before the onset of budding, remaining associated with the bud neck up to the point of cell division (**Figure 4B**). A very similar behavior was observed for a BacD variant fused to the yellow fluorescent protein Venus (Nagai et al., 2002) (**Figure 4C**), consistent with the notion that the two bactofilin paralogs interact. In support of this hypothesis, studies of a strain in which both proteins were fluorescently labeled showed that BacA and BacD indeed co-localized to a large extent during all stages of the developmental cycle (**Figure 4D** and **Figure 4—figure supplement 3**). However, at the onset of bud formation, the signals of the two proteins were not always fully superimposable, with BacD assemblies occasionally detectable both at the bud neck and in the mother cell (**Figure 4—figure supplement 4**). In the absence of BacA, BacD-Venus still formed distinct foci, albeit at apparently random positions within the cell (**Figure 4—figure supplement 5**). Notably, a BacA-YFP variant carrying a previously reported mutation that disrupts the polymerization interface (F130R) (Deng et al., 2019; Vasa et al., 2015; Zuckerman et al., 2015) was evenly distributed within the cell and unable to functionally replace the wild-type protein, indicating that the formation of polymeric assemblies is essential for proper BacA localization and function (**4—figure supplement 6**). Given that the bactofilin assemblies are localized to the stalk and bud boundaries and required to prevent unconstrained growth of these cellular structures, we hypothesized that the bactofilin cytoskeleton might serve to limit the cell wall biosynthetic machinery to the different growth zones of *H. neptunium*.

To further investigate the role of bactofilin in the spatial regulation of cell wall biosynthesis, we generated derivatives of the wild-type and Δ*bacAD* strains that produced a fluorescently (YFP-) labeled variant of the membrane-bound elongasome protein RodZ, a core structural component of the complex connecting the cytoplasmic MreB cytoskeleton to the periplasmic enzymatic machinery (Bendezú et al., 2009; van den Ent et al., 2010; Alyahya et al., 2009). In the wild-type background, RodZ-YFP formed dynamic foci in in the mother cell, at the (incipient) stalk base

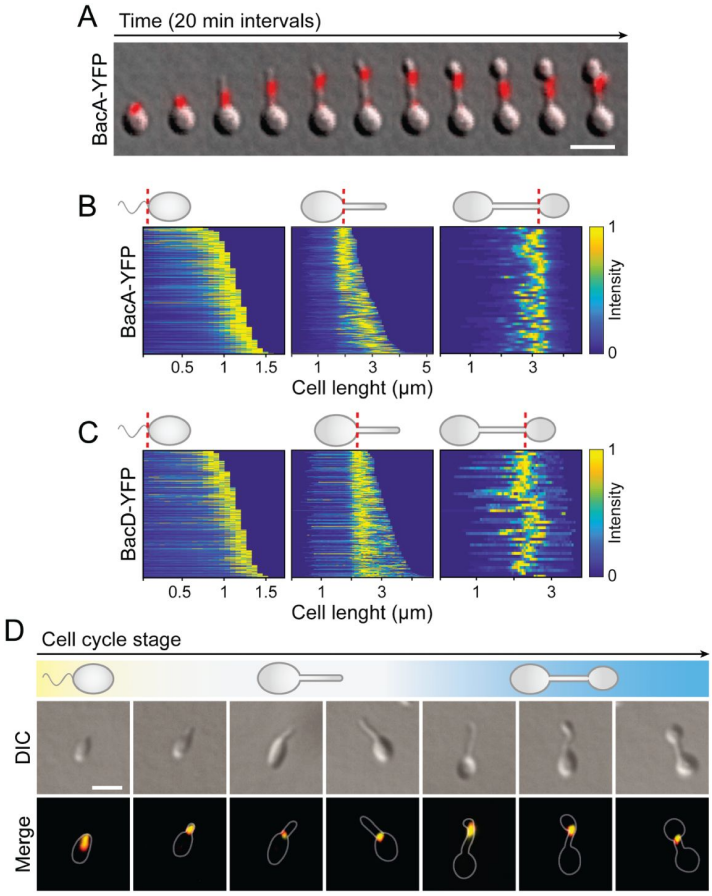

Figure 4.

BacA and BacD show a dynamic, cell cycle-dependent localization pattern.

(A) Localization pattern of BacA-YFP. Cells of strain EC61 (*bacA*::*bacA-eyfp*) were transferred to agarose pads and imaged at 20-min intervals. Shown are overlays of DIC and fluorescence images of a representative cell, with YFP fluorescence shown in red. Scale bar: 3 µm. **(B)** Demographic analysis of BacA-YFP localization in swimmer (left), stalked (middle), and budding (right) cells of strain EC61 (*bacA*::*bacA-eyfp*). The fluorescence intensity profiles measured for cells of each type were sorted according to cell length and stacked on each other, with the shortest cell shown at the top and the longest cell shown at the bottom (n=250 swimmer cells, 215 stalked cells and 49 budding cells). Dotted red lines indicate the positions to which cells were aligned. **(C)** Demographic analysis of BacD-Venus localization. Cells of strain EC67 (*bacD*::*bacD-venus*) were analyzed as described in panel B (n=416 swimmer cells, 248 stalked cells and 45 budding cells). **(D)** Co-localization of BacA and BacD in cells of strain EC68 (*bacA*::*bacA-eyfp bacD*::*bacD-mCherry*). Shown are DIC images and overlays of the YFP and mCherry signals of representative cells, arranged according to their developmental state. The individual signals are shown in **Figure S6A**. The Pearson's Correlation Coefficient (PCC) of the two fluorescence signals in a random population of cells (n=454) is 0.506. Bar: 1 µm.

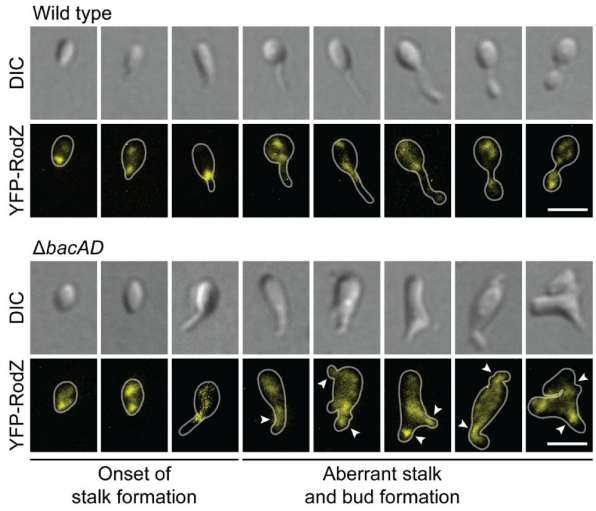

Figure 5.

The bactofilin cytoskeleton is required to confine the elongasome to the mother cell and bud compartments.

Localization of eYFP-RodZ in the *H. neptunium* wild-type and Δ*bacAD* backgrounds. Shown are representative cells of strain EC93 (*rodZ*::*eyfp-rodZ*) and SP221 (Δ*bacAD rodZ*::*eyfp-rodZ*) imaged by DIC and fluorescence microscopy and arranged according to their developmental state. Arrowheads indicate cellular extensions that show eYFP-RodZ foci. Bar: 2 µm.

Figure 5—video 1. Localization of YFP-RodZ during stalk synthesis in the wild-type background. Cells of strain EC93 (*rodZ*::*eyfprodZ*) were immobilized on pads made of 1% agarose in ASS medium and imaged at 2 min intervals. Bar: 2 µm.

Figure 5—video 2. Localization of YFP-RodZ during bud formation in the wild-type background. Cells of strain EC93 (*rodZ*::*eyfprodZ*) were immobilized on pads made of 1% agarose in ASS medium and imaged at 2 min intervals. Bar: 2 µm.

Figure 5—video 3. Localization of YFP-RodZ during pseudo stalk synthesis in the Δ*bacAD* background. Cells of strain SP221 (Δ*bacAD rodZ*::*eyfp-rodZ*) were immobilized on pads made of 1% agarose in ASS medium and imaged at 2 min intervals. Bar: 2 µm.

Figure 5—video 4. Localization of YFP-RodZ within within early stalks in the Δ*bacAD* background. Cells of strain SP221 (Δ*bacAD rodZ*::*eyfp-rodZ*) were immobilized on pads made of 1% agarose in ASS medium and imaged at 2 min intervals. Bar: 2 µm.

Figure 5—video 5. Localization of YFP-RodZ in amorphous cells in the Δ*bacAD* background. Cells of strain SP221 (Δ*bacAD rodZ*::*eyfp-rodZ*) were immobilized on pads made of 1% agarose in ASS medium and imaged at 2 min intervals. Bar: 2 µm.

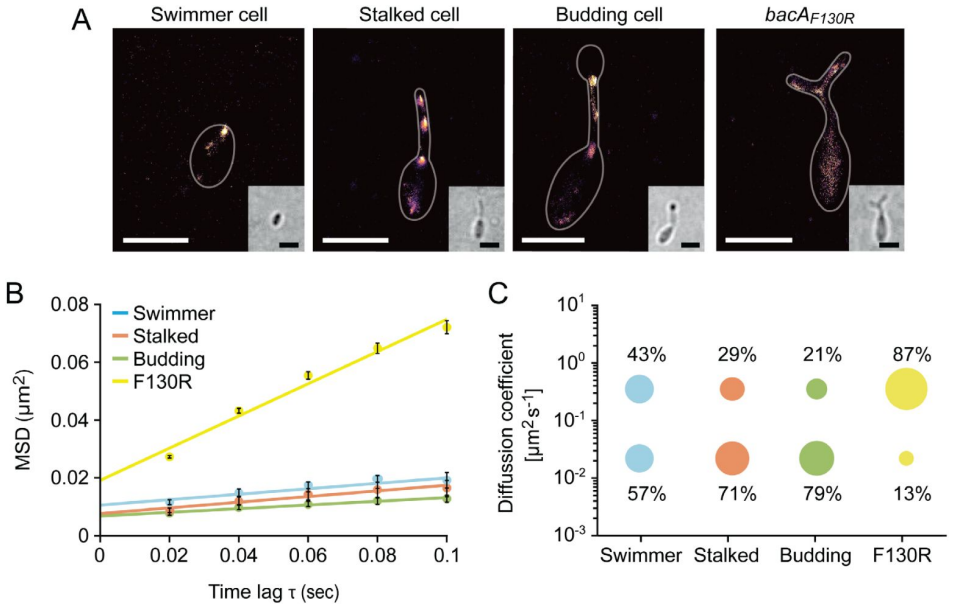

Figure 6.

The single-particle dynamics of BacA change over the course of the cell cycle.

(A) Representative heat maps showing the sum of single-particle positions observed in live-cell single-particle localization microscopy studies of a swimmer, stalked and budding cell producing BacA-YFP (EC61) or a mutant cell producing the polymerization-deficient BacAF130R-YFP variant (MO78). Insets show the corresponding bright-field images. Bars: 1 µm. **(B)** Mean-squared displacement (MSD) analysis of the mobility of BacA-YFP in wild-type swimmer (n=100), stalked (n=105) and budding (n=101) cells (EC61). Cells (n=110) producing the BacAF130RYFP were analyzed as a control (MO78). Error bars indicate the standard deviation. **(C)** Bubble plots showing the proportions of mobile and immobile particles (size of the bubbles) and the corresponding average diffusion constants (y-axis) in the cells analyzed in panel B.

Figure 6—video 1. Tracking of single BacA-YFP particles in representative cells at different stages of the cell cycle. Shown are stream acquisitions (20-ms intervals) of *H. neptunium* cells producing wild-type BacA-YFP (EC61) or the polymerization-deficient BacAF130R-YFP variant (MO78) in place of the native BacA protein at different developmental stages. Bar: 1 µm

and the nascent bud (**Figure 5** and **Figure 5—videos 1,2**), thus localizing to the different growth zones detected by HADA labeling (**Figure 2C**). These results are in line with previous findings identifying the elongasome as a key determinant of cell growth in *H. neptunium* (Cserti et al., 2017). Importantly, however, RodZ-YFP foci were never observed in the stalk, suggesting that elongasome complexes are unable to cross the stalk base and the bud neck, even though their free components appear to be able to diffuse through the stalk to facilitate the *de novo* assembly of elongasomes in the incipient bud compartment. In the Δ*bacAD* mutant, the localization behavior of RodZ-YFP resembled that in the wild-type background as long as the cells were the early stages of the cell cycle, with dynamic foci detectable throughout the cell envelope and at the (future) stalk base (**Figure 5** and **Figure 5—video 3**). However, at later stages, the elongasome was no longer excluded from the nascent stalk structure and, in many cases, even appeared to be enriched this region, leading to its remodeling into an increasingly amorphous cellular extension (**Figure 5** and **Figure 3—videos 3-5**). The bactofilin cytoskeleton itself or the high degree of positive inner cell curvature induced in its presence at the stalk base thus appear to act as a barrier that excludes elongasome complexes from the stalk and thus facilitates proper morphogenesis and bud development.

The assembly state of BacA changes at different stages of *H. neptunium* development

Since bactofilins form highly stable polymers *in vitro* (Kühn et al., 2010; Zuckerman et al., 2015), the dynamic localization observed for BacA and BacD was unexpected. To further characterize the dynamics of the bactofilin cytoskeleton in *H. neptunium*, we followed the movement of individual BacA-YFP molecules in swimmer, stalked and budding cells (**Figure 6—video 1**). First, we used single-molecule tracking data to generate high-resolution images of the bactofilin assemblies in each of the three cell types. The results confirmed the cell cycle-dependent localization patterns observed by widefield fluorescence microscopy (**Figure 6A** and **Figure 6—figure supplement 1**). In addition, they revealed clusters in medial regions of the stalk, which may represent transient polymers formed during the reshuffling of bactofilin molecules between the stalk base and the (incipient) bud neck. When calculating the average mean squared displacement of the tracked BacA-YFP molecules, we found that their mobility decreased gradually from the swimmer over the stalked cell to the budding cell stage (**Figure 6B**). For each cell type, the distribution of step sizes in the single-particle tracks suggests the existence of two distinct diffusion regimes, with a static (D= 0.02 ± 0.0004 $\mu m^2 s^{-1}$) and a mobile (D= 0.35 ± 0.004 $\mu m^2 s^{-1}$) population, likely representing the polymerized and freely diffusible states, respectively (**Figure 6C** and **Figure 6—figure supplement 2**). In swimmer cells, the static fraction comprised only ~60% of the molecules. Its proportion increased to ~70% in stalked cells and finally reached ~80% in budding cells. The F130R variant, by contrast, showed less than 15% of static molecules (**Figure 6B,C** and **Figure 6—figure supplement 2** and **Figure 6—video 1**) consistent with the notion that it is impaired in polymerization but still able to assemble under certain conditions after undergoing a structural change that generates an alternative polymerization interface (Deng et al., 2019). Collectively, these results show that, in *H. neptunium*, the assembly state of the bactofilin cytoskeleton changes as cells progress through their developmental cycle. Moreover, despite the inherent stability of bactofilin polymers, all cell types display a sizeable fraction of mobile BacA-YFP molecules, which could potentially reflect the dynamic reorganization of bactofilin assemblies during cell growth.

Bactofilin genes are often clustered with genes encoding M23 peptidases

After identifying a critical role of BacA in *H. neptunium* morphogenesis, we set out to gain further insight into its mechanism of action. Notably, in several species in which bactofilins play a role in cell shape determination, the corresponding bactofilin genes are located adjacent to genes encoding a putative M23 peptidase homologous to LmdC (**Figure 7A**). To determine whether this

gene arrangement was more widely conserved, we performed a comprehensive bioinformatic analysis in which we searched all bacterial genome sequences available for putative bactofilin genes that were located immediately upstream or downstream of open reading frames encoding proteins with a predicted M23 peptidase domain. This analysis identified a total of 226 species from a wide variety of bacterial phyla (**Figure 7B** and **Figure 7— Dataset 1**), suggesting a conserved functional association between bactofilins and M23 peptidases.

The M23 peptidase LmdC of *H. neptunium* has peptidoglycan hydrolase activity *in vitro*

Like many of its homologs, *H. neptunium* LmdC is a predicted bitopic membrane protein with a short N-terminal cytoplasmic region, a transmembrane helix, large periplasmic region composed of a predicted coiled-coil domain, and a C-terminal M23 peptidase domain (**Figure 8A**). Members of the M23 peptidase family usually have Zn^{+}-dependent hydrolase activity and cleave bonds within the peptide side chains of in the peptidoglycan meshwork (Firczuk et al., 2005; Grabowska et al., 2015). However, there are also various representatives that have lost their enzymatic activity because of mutations in residues required for metal cofactor binding and have instead adopted regulatory roles in cell wall biosynthesis (Figueroa-Cuilan et al., 2021; Goley et al., 2010; Gurnani Serrano et al., 2021; Möll et al., 2010; Poggio et al., 2010; Uehara et al., 2010). An amino acid alignment showed that the M23 peptidase domain of LmdC features all residues reported to be critical for Zn^{2+} binding, suggesting that it could act as a genuine peptidoglycan hydrolase (**Figure 8B**). In a structural model of LmdC generated with AlphaFold2 (Jumper et al., 2021), the periplasmic coiled-coil and M23 peptidase domains form an elongated, rigid unit with two flanking non-structured regions that is flexibly linked to the transmembrane helix (**Figure 8C**). Notably, LmdC homologs were shown to form a distinct clade among the M23 peptidases that is broadly conserved among species but particularly enriched in alpha- and deltaproteobacteria (Figueroa-Cuilan et al., 2021).

To clarify whether LmdC was indeed catalytically active, we purified a C-terminal fragment of the protein including the M23 peptidase domain and assayed its activity *in vitro*. Peptidoglycan from *H. neptunium* shows only a low degree of cross-linkage and hardly any pentapeptides (Cserti et al., 2017), likely due to a high level of autolytic activity. We therefore used normally crosslinked, pentapeptide-enriched peptido-glycan from *E. coli* strain D456 (lacking PBPs 4, 5 and 6) (Edwards and Donachie, 1993) as a substrate to enable a comprehensive analysis of the cleavage specificity of LmdC. Upon treatment with the protein, the proportion of dimeric muropeptide species strongly decreased, regardless of the length of the cross-linked peptides and without the formation of major additional monomer peaks (**Figure 8D**). The activity of LmdC was particularly high at a pH value of 5, but the physiological significance of this effect remains to be determined. Collectively, these results demonstrate that LmdC is a DD-endopeptidase cleaving the bond between the meso-diaminopimelic acid residue of one peptide and D-alanine at position 4 of the other peptide, thereby reducing the degree of cross-linkage within the peptidoglycan layer (**Figure 8E**).

LmdC is critical for morphogenesis in *H. neptunium* and physically interacts with BacA

To clarify whether LmdC was also required for proper growth in *H. neptunium*, we aimed to generate a mutant strain lacking LmdC activity. However, all attempts to delete the *lmdC* gene or the entire putative *lmdC-bacA* operon or to generate non-functional truncated *lmdC* alleles were unsuccessful, in line with a previous report suggesting that *lmdC* is essential for viability (Cserti et al., 2017). It was also not possible to generate a conditional *lmdC* mutant producing the gene under the control of a copper-inducible promoter, suggesting that its expression level needs to be precisely regulated.

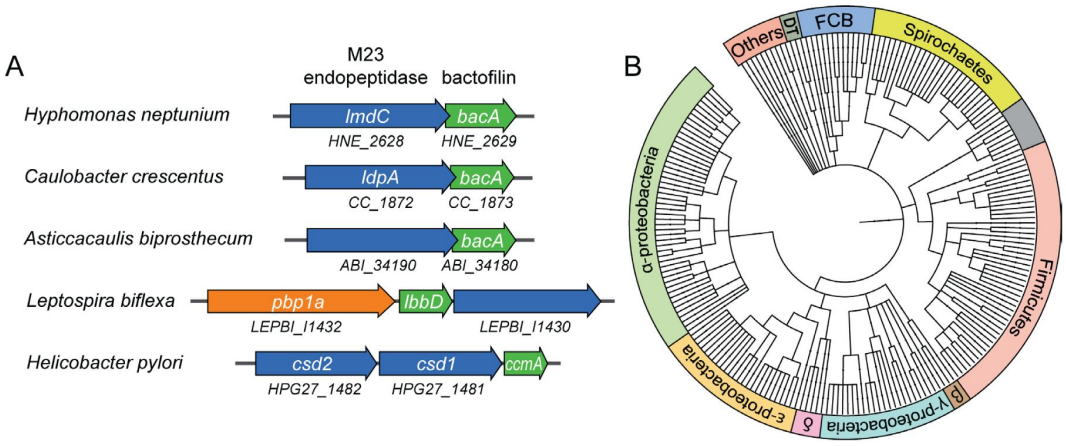

Figure 7.

Putative operons comprising adjacent BacA and M23 peptidase genes are widely conserved among bacteria.

(A) Arrangement of *bacA* and *lmdC* genes in species whose BacA homolog has a proven role in cell morphogenesis. **(B)** Co-conservation of BacA and M23 peptidase genes across different bacterial phyla. Bioinformatic analysis was used to identify genomes that contained a bactofilin gene located next to an M23 peptidase gene. After retrieval of the taxonomy IDs of the corresponding species from the National Center for Biotechnology Information (NCBI) website, a phylogenetic tree of the species was created using the iTOL server (Letunic and Bork, 2021). Abbreviations: DT (Deinococcus-Thermus group), FCB (Fibrobacteres-Chlorobi-Bacteroidetes group), β (β-proteobacteria), δ (δ-proteobacteria). The full list of species used and details on the genes identified are provided in **Figure 7—Dataset 1**.

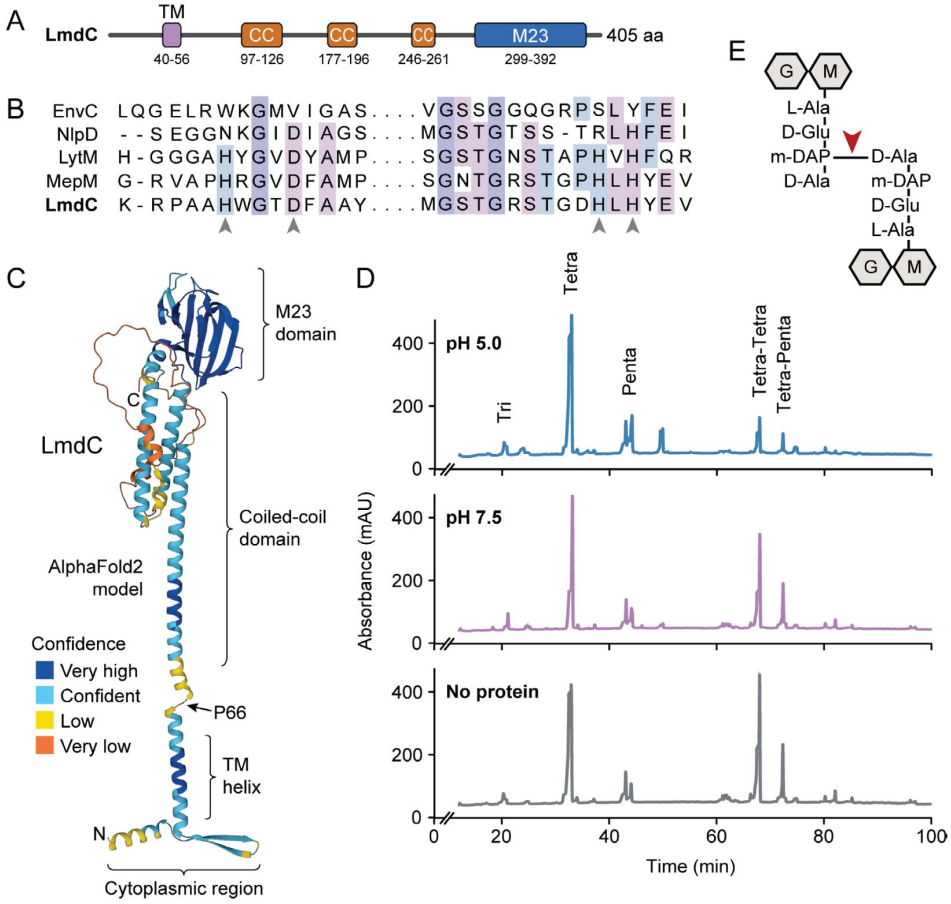

Figure 8.

LmdC is a peptidoglycan hydrolase with DD-endopeptidase activity.

(A) Predicted domain architecture of *H. neptunium* LmdC. The predicted positions of the transmembrane helix (TM), the three coiled-coil regions (CC) and the M23 peptidase domain are indicated. **(B)** Alignment of the amino acid sequences of multiple M23 peptidases showing the conservation of the catalytic residues in LmdC. Residues required to coordinate the catalytic Zn^{2+} ion of LytM from *S. aureus* (Firczuk et al., 2005) are indicated by arrowheads. The proteins shown are EnvC from *E. coli* (UniProt: P37690), NlpD from *E. coli* (P0ADA3), LytM from *S. aureus* (O33599), MepM from *E. coli* (P0AFS9) and LmdC from *H. neptunium* (Q0BYX6). **(C)** Predicted molecular structure of *H. neptunium* LmdC, generated with Alphafold2 (Jumper et al., 2021). The different domains of the protein and the position of proline 66, which terminates the N-terminal fragment of LmdC used for the *in vivo* analyses in this study (LmdC1-66) are indicated. **(D)** HPLC traces showing the muropeptide profile of peptidoglycan treated with LmdC. Cell walls were incubated with the isolated M23 peptidase domain of LmdC at pH 5.0 and pH 7.5. Subsequently, muropeptides were released with cellosyl, reduced and separated by HPLC. A control sample lacked LmdC (No protein). The nature of the major products is indicated above the peaks. Tri, Tetra and Penta stand for N-acetylglucosamine-N-acetylmuramitol tripeptide, tetrapeptide and pentapeptide, respectively. **(E)** Structure of a TetraTetra muropeptide. Abbreviations: G (N-acetylglucosamine), M (N-acetylmuramic acid). The cleavage site of LmdC is indicated by a red arrowhead.

To address this issue, we developed a CRISPR interference (CRISPRi) system (Larson et al., 2013) that enabled the inducible down-regulation of target genes in *H. neptunium*. It is based on a newly constructed integrative plasmid (pdCas9Entry) that carries the gene for a nuclease-deficient variant of *Streptococcus pyogenes* Cas9 (dCas9) under the control of a copper-inducible promoter as well as a cassette for the construction and constitutive expression of a gene-specific small guide RNA (sgRNA) (**Figure 9A** and **Figure 9—figure supplement 1A**). A derivative of this plasmid encoding an sgRNA directed against the 5' region of the *lmdC* gene was then inserted into the *H. neptunium* chromosome (**Figure 9B**). Induction with copper led to the formation of an sgRNA-dCas9 complex that targeted the non-coding strand of *lmdC*, generating a road-block that prevented the movement of RNA polymerase and, thus, gene expression (**Figure 9C,D**). Importantly, the block of *lmdC* expression led to cell shape defects very similar to those observed for the Δ*bacA* mutant, as reflected by a large proportion of distorted and amorphous cells, which still showed close-to-normal growth rates (**Figure 9E,F** and **Figure 9—figure supplement 1B,C**). Induced cells of a control strain carrying the empty pdCas9Entry plasmid did not show any obvious phenotype, indicating that the presence of dCas9 alone did not have any adverse effects on cell growth or viability (**Figure 9D,E** and **Figure 9—figure supplement 1C**). These results suggest that LmdC and BacA are part of the same morphogenetic pathway.

To further investigate whether the peptidoglycan hydrolase LmdC was functionally linked to bactofilins in *H. neptunium*, we aimed to conduct *in vivo* co-localization studies. However, all attempts to generate functional fluorescent protein fusion to full-length or C-terminally truncated LmdC failed, because the fusion proteins were either unstable or did not produce any fluorescence signal *in vivo*. As a complementary approach, we analyzed the interaction between LmdC and BacA *in vitro* by biolayer interferometry. To this end, a synthetic peptide comprising the predicted cytoplasmic region of LmdC (amino acids 1-38) was immobilized on a biosensor and probed with increasing concentrations of purified BacA protein. The results showed that BacA interacts with the LmdC peptide with an apparent equilibrium dissociation constant (K_D) of ~15 µM. By contrast, an unrelated peptide used as a negative control was not bound with appreciable affinity (**Figure 9G,H**). This result confirms a direct interaction between BacA and LmdC and identifies the N-terminal cytoplasmic region of LmdC as the interaction determinant for BacA association.

R. rubrum BacA recruits LmdC to the inner curve of the cell to modulate cell curvature

Our bioinformatic analysis suggests that bactofilins and M23 peptidases may be functionally associated in a large number of species. To further explore this possibility, we turned our efforts to the spiral-shaped bacterium *Rhodospirillum rubrum*, which contains a putative *lmdC-bacA* operon similar to that in *H. neptunium* (Munk et al., 2011) (**Figure 10A**). The *R. rubrum* BacA homolog Rru_A1867 ($BacA_{Rs}$) is 37% identical (57% similar) to BacA of *H. neptunium* and also consists of a central Bactofilin A/B domain flanked by terminal non-structured regions (**Figure 10B**). The LmdC homolog Rru_A1868 ($LmdC_{Rs}$) is 39% identical (55% similar) to *H. neptunium* LmdC and has a similar predicted molecular structure (Varadi et al., 2022). The deletion of $bacA_{Rs}$ led to a noticeable increase in cell curvature (**Figure 10C** and **Figure 10—figure supplement 1A**), as also reflected in a significant increase in cell sinuosity (**Figure 10D**). A very similar effect was observed for cells lacking $lmdC_{Rs}$ or both $bacA_{Rs}$ and $lmdC_{Rs}$, indicating that the two gene products act in the same pathway and jointly contribute to cell shape maintenance in *R. rubrum* (**Figure 10C,D and Figure 10—figure supplement 1A**). In the two mutant strains, the global composition of peptido-glycan was largely unchanged, supporting the notion that the $BacA_{Rs}$-$LmdC_{Rs}$ pathway modifies the cell wall only locally or acts by modulating the activity of the standard cell elongation machinery (**Figure 10— figure supplement 1B**).

Complementation studies showed that the expression of a plasmid-borne copy of *bacA* under the control of a weak constitutive promoter attenuated the curvature defect, albeit only partially, likely due to inade-quate expression levels (**Figure 10—figure supplement 2**). The generation of

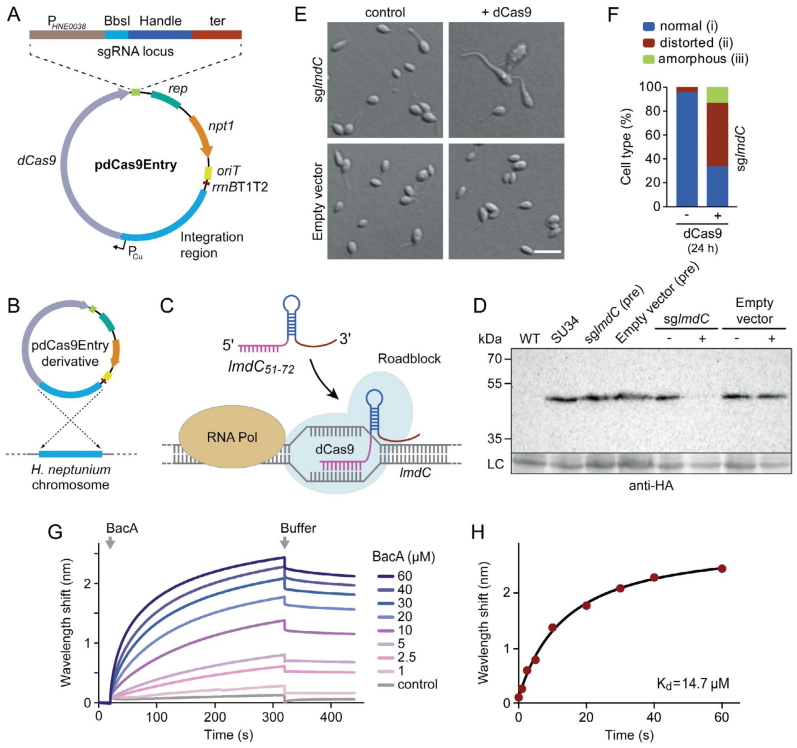

Figure 9.

LmdC interacts with BacA to mediate *H. neptunium* morphogenesis.

(A) Schematic representation of the integrative plasmid pdCas9Entry, enabling CRISPR interference (CRISPRi) in *H. neptunium*. The plasmid harbors a chromosomal fragment containing the copper-inducible PCu promoter, followed by a gene encoding a nuclease-deficient variant of Cas9 (dCas9). It also contains an sgRNA expression cassette composed of the constitutive P*HNE0038* promoter, a BbsI cloning site for the insertion of target-specific DNA fragments, a sequence encoding the sgRNA handle and a transcriptional terminator (ter). Other features of the plasmid are a replication initiator gene (*rep*), a kanamycin resistance gene (*npt1*), an origin of transfer (*oriT*) and a strong transcriptional terminator (*rrnB*T1T2) that is placed upstream of the PCu-containing fragment. The DNA sequence of the sgRNA expression cassette is given in **Figure 9–figure supplement 1**. **(B)** Schematic showing the integration of a pdCas9Entry derivative into the *H. neptunium* chromosome by single homologous recombination at the PCu locus. **(C)** Mechanism of the CRISPRi-mediated repression of *lmdC* expression. In the presence of inducer, dCas9 interacts with a constitutively produced sgRNA that targets bases 51-72 of the non-coding strand of *lmdC* (sg*lmdC*). The formation of the interference complex creates a roadblock that blocks the transcription of *lmdC* by RNA polymerase. **(D)** Immunoblot analysis verifying the CRISPRi-mediated depletion of LmdC. Strain SU34 (*lmdC*::*lmdC-HA*), which produces a fully functional variant of LmdC carrying the HA affinity tag inserted in between the transmembrane helix and the coiled-coil domain, was transformed with pdCas9Entry (empty vector) or plasmid pJH13 (sg*lmdC*). The resulting strains (SP249 and SP236) were grown for 24 h in the absence (-) or presence (-) of 0.3 mM CuSO4 and subjected to immunoblot analysis with an anti-HA antibody. The wild-type strain (LE670), the parental strain SU34 as well as the uninduced pre-cultures (pre) of strains SP249 and SP236 used for the experiment were analyzed as controls. A non-specific band served as a loading control (LC). **(E)** Morphology of *H. neptunium* cells depleted of LmdC. Shown are representative cells of strains SP236 (*lmdC*::*lmdC*-HA pJH13) (sg*lmdC*) and SP249 (*lmdC*::*lmdC*-HA pCas9Entry) (empty vector) grown for 24 h in the absence (control) or presence (+ dCas9) of 0.3 mM CuSO4. Cells were imaged by DIC and fluorescence microscopy. Bar: 2 μm. **(F)** Quantification of the proportion of phenotypically abnormal stalked and budding cells in the cultures of strain SP236 (*lmdC*::*lmdC*-HA pJH13) analyzed in panel E (n=100 cells per condition). **(G)** Bio-layer interferometric analysis of the interaction between cytoplasmic domain of LmdC and BacA. Sensors derivatized with a biotinylated synthetic peptide comprising the N-terminal cytoplasmic region of LmdC (amino acids 1-38) were probed with the indicated concentrations of BacA. After the association of BacA, the sensors were transferred to protein-free buffer to induce BacA dissociation. The interaction kinetics were followed by monitoring the wavelength shifts resulting from changes in the optical thickness of the sensor surface during association or dissociation of the analyte. The extent of non-specific binding of BacA to the sensor surface was negligible (control). **(H)** Affinity of the BacA-LmdC interaction. The maximal wavelength shifts measured in the experiment shown in panel D were plotted against the corresponding BacA concentration. The data were fitted to a one-site binding model, yielding an apparent *K*d value of ~15 μM.

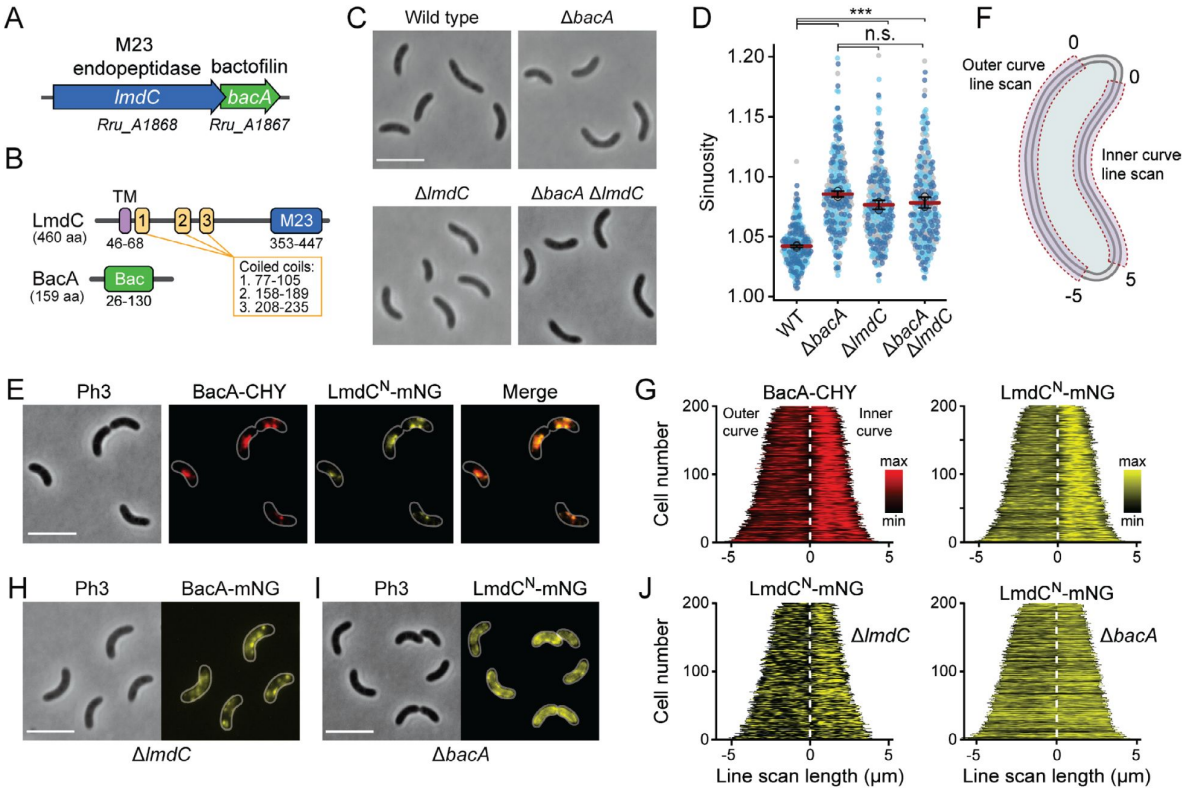

Figure 10.

BacA and LmdC contribute to cell morphogenesis in *R. rubrum*.

(A) Schematic representation of the *bacA-lmdC* operon in *R. rubrum*. **(B)** Domain organization of LmdC and BacA from *R. rubrum*. LmdC consists of a transmembrane helix (TM) followed by a coiled-coil-rich region and a C-terminal M23 peptidase domain (M23). The bactofilin polymerization domain (green box) is flanked by non-structured N- and C-terminal regions. Numbers indicate the first and last amino acid of a domain. **(C)** Phenotypes of *R. rubrum* wild-type (S1), Δ*bacARs* (SP70), Δ*lmdCRs* (SP68) and Δ*bacARs* Δ*lmdCRs* (SP116) cells, imaged using phase-contrast microscopy. Bar: 5 µm. **(D)** Superplots showing the distribution of cell sinuosities in populations of the indicated *R. rubrum* strains. Small dots represent the data points, large dots represent the median values of the three independent experiments shown in the graphs (dark blue, light blue, grey). The mean of the three median values is indicated by a horizontal red line. Whiskers represent the standard deviation. *** p<0.005; ns, not significant; t-test). **(E)** Co-localization of BacA*Rs*-CHY and LmdC^{N}*Rs*-mNG in the Δ*lmdCRs* background (SP119). The Pearson's Correlation Coefficient (PCC) of the two fluorescence signals in a random subpopulation of cells is 0.916. Scale bar: 5 µm. **(F)** Schematic showing the approach used to quantify the distribution of proteins along the outer and inner curve of a cell in panel G. **(G)** Demographs showing the enrichment of BacA-CYH and LmdC^{N}-mNG at the inner curve the populations of strain SP119 analyzed in panel E (n=200 per strain). The white dashed line represents the point of transition from the outer to the inner curve. **(H)** Localization of BacA*Rs*-mNG in the Δ*lmdCRs* background (SP98). Bar: 5 µm. **(I)** Localization of LmdC*Rs*-mNG in the Δ*bacARs* background (SP118). Bar: 5 µm. **(J)** Demographs showing the outer-versus-inner curve distribution of BacA*Rs*-mNG in the Δ*lmdCRs* background (SP98; n=200) and LmdC^{N}*Rs*-mNG in the Δ*bacARs* background (SP118; n=200). The white dashed line represents the point of transition from the outer to the inner curve.

an analogous plasmid to complement the deletion of *lmdC*$_{Rs}$ failed, because it was not possible to introduce the construct into *Escherichia coli* for plasmid propagation, suggesting that the expression of *lmdC*$_{Rs}$ was toxic to the cells. To further test this hypothesis, we constructed a plasmid enabling the expression of the gene under a tightly controlled, inducible promoter in *E. coli*. Upon induction, a large part of the cell population lyzed, whereas control cells carrying an empty plasmid did not show any phenotypic defects (**Figure 10—figure supplement 3**). These results indicate that, similar to its *H. neptunium* homolog, LmdC$_{Rs}$ is an active enzyme with peptidoglycan hydrolase activity.

To further test the hypothesis that LmdC was functionally linked to bactofilin in *R. rubrum*, we set out to perform *in vivo* co-localization studies. However, all attempts to generate fluorescently labeled variants of full-length LmdC failed, because the corresponding *R. rubrum* expression plasmids appeared to be toxic to *E. coli*. Importantly, our *in vitro* studies had shown that the interaction of LmdC with the bactofilin cytoskeleton was mediated by its N-terminal cytoplasmic region (**Figure 9G,H**). To avoid the issues caused by the full-length protein, we therefore generated a reporter fusion encoding only the predicted N-terminal cytoplasmic region and the transmembrane helix (amino acids 1-80) of LmdC$_{Rs}$ fused to the green fluorescent protein mNeonGreen (Shaner et al., 2012) (LmdC$^{N}_{Rs}$-mNG) (**Figure 10—figure supplement 4A-C**). A low-copy plasmid carrying the corresponding allele under the control of the native *lmdC*$_{Rs}$ promoter was then introduced into an *R. rubrum* Δ*lmdC*$_{Rs}$ mutant producing a fully functional fusion of BacA$_{Rs}$ to the red fluorescent protein mCherry (BacA$_{Rs}$-CHY) (Shaner et al., 2004) in place of the wild-type protein (**Figure 10—figure supplement 2**). We found that BacA$_{Rs}$-CHY and LmdC$^{N}_{Rs}$-mNG were consistently localized to the same subcellular positions, forming patchy or filamentous structures that were preferentially, but not exclusively, positioned at the inner curve of the cell (**Figure 10E**). A very similar behavior was observed in the presence of wild-type LmdC$_{Rs}$ (**Figure 10—figure supplement 4D**). To further validate the enrichment of the two fusion proteins at the inner curve, we quantified their fluorescence signals along the inner and outer curves of multiple individual cells, concatenated the resulting fluorescence profiles and ordered them according to their total length. In both cases, cells consistently displayed higher signal intensities at the inner curve (**Figure 10F,G**), supporting the notion that BacA$_{Rs}$-LmdC$_{Rs}$ assemblies promote cell wall biosynthesis in the inner curve to reduce overall cell curvature. Notably, a BacA$_{Rs}$-mNG fusion showed a reduced enrichment in the absence of LmdC$_{Rs}$, whereas LmdC$^{N}_{Rs}$-mNG completely lost its asymmetric distribution in the Δ*bacA*$_{Rs}$ background (**Figure 10H-J**). These results identify BacA$_{Rs}$ polymers as recruitment platforms for LmdC$_{Rs}$, although an interaction between the two proteins appears to be required for normal BacA$_{Rs}$ localization.

LmdC recruitment depends on the conserved cytoplasmic β-hairpin motif

The N-terminal cytoplasmic region of LmdC$_{Rs}$ contains a β-hairpin motif (**Figure 11A**) that is conserved among LmdC homologs. To determine whether this structural feature was involved in BacA binding, we exchanged two small clusters of amino acids that protruded from its surface and might thus serve as interaction determinants, using LmdC$^{N}_{Rs}$-mNG as a reporter. Cluster I (R25, H26, L27) was located within the first β-strand, whereas cluster II (R30, S31) was close to the β-turn (**Figure 11B**). The modifications in cluster I completely abolished the enrichment of LmdC at the inner curve of the cell, indicating that the β-hairpin motif is a critical part of the BacA binding site (**Figure 11C,D**). Notably, the loss of interaction between the two proteins also led to a reduced inner-curve enrichment of BacA$_{Rs}$-CHY, as previously observed in the Δ*lmdC*$_{Rs}$ background (**Figure 10I,J**). This observation confirms that LmdC$_{Rs}$ binding is required for BacA to adopt its proper spatial organization. Similar defects were caused by the modification of cluster II (**Figure 11C,E**). However, in this case, BacA$_{Rs}$-CHY was also no longer enriched at the inner curve, suggesting that the mutant protein may still show a residual, yet aberrant interaction with BacA$_{Rs}$ that has a negative effect on BacA$_{Rs}$ localization. Collectively, these findings confirm a functional

association between the bactofilin cytoskeleton and LmdC$_{Rs}$ in *R. rubrum*. Moreover, they support the notion that bactofilins and LmdC-like M23 peptidases form a conserved morphogenetic module that is involved in the establishment of complex bacterial cell shapes.

Discussion

Although bactofilins are widely conserved among bacteria, their cellular functions are still incompletely understood. Here, we show that BacA homologs critically contribute to cell shape determination in two morphologically distinct members of the alphaproteobacteria, the stalked budding bacterium *H. neptunium* and the spiral-shaped bacterium *R. rubrum*. In both cases, they functionally interact with LmdC-type DD-endopeptidases to promote local changes in the pattern of peptidoglycan biosynthesis. Bactofilins thus complement the activities of the MreB and FtsZ cytoskeletons in the regulation of cell growth and act as versatile cell shape modifiers that facilitate the establishment of complex bacterial morphologies.

In *H. neptunium*, the bactofilin cytoskeleton localizes dynamically to the stalk base and the bud neck, promoting stalk growth and subsequent bud formation (**Figure 4**). While flanked by zones of active growth, the stalk itself is usually devoid of cell wall biosynthetic machinery (Cserti et al., 2017) (**Figure 5**). In bactofilin-deficient cells, however, the stalk and bud growth zones are no longer confined and expand into the stalk envelope, leading to stalk widening and the formation of irregular bulges due to uncontrolled peptidoglycan incorporation and bud expansion (**Figure 2** and **Figure 5**). Bulges or larger amorphous segments at some point separate from the mother cell and then continue to grow as independent cells, indicating that chromosome replication and segregation as well as cell division still occur under these conditions. Together, these observations suggests that bactofilin polymers establish barriers that normally prevent the entry of elongasome complexes from the mother cell or nascent bud compartments into the stalk.

The precise mechanism underlying the function of bactofilin in cell morphogenesis remains to be clarified. It is conceivable that bactofilin polymers act by tethering peptidoglycan biosynthetic proteins or establishing physical barriers that hinder the mobility of elongasome complexes (**Figure 12A**). However, we observed a close functional association of bactofilins with M23 peptidases that appears to be widely conserved among species, suggesting that their activity may be intimately tied to cell wall hydrolysis. The transition zones between the stalk and the adjacent mother cell and bud compartments are characterized by a high degree of positive inner cell curvature, which is in stark contrast to the negative curvature in the remaining parts of the cell. The hydrolytic activity of *H. neptunium* LmdC may be critical to remodel the cell wall in these zones and thus facilitate the extrusion of the stalk. Importantly, MreB is thought to move along regions of negative inner cell curvature (Hussain et al., 2018; Wong et al., 2019). The positively curved transition zones generated by the bactofilin-LmdC assemblies could therefore represent topological barriers that are difficult to cross by elongasome complexes, thereby helping to restrict their movement to the mother cell and bud compartments. Moreover, the narrow diameter stalks and their exceedingly high degree of negative inner cell curvature may reduce the stability of elongasome complexes that may form spontaneously in the stalk region. These effects may also be important during the stalk elongation phase following cell division, when bactofilin assemblies are no longer present at the stalk base.

Notably, a role in stalk formation has also been reported for the bactofilin homologs of *C. crescentus* and *A. biprosthecum*. In *C. crescentus*, the major bactofilin BacA was shown to act as a localization determinant for the bifunctional penicillin-binding protein PbpC, a cell wall synthase that contributes to stalk elongation (Kühn et al., 2010) and the proper sorting of a stalk-specific protein (Hughes et al., 2013). However, the absence of BacA only leads to a moderate reduction in stalk length and leaves overall cell shape unaffected, indicating that this protein has only a minor role in *C. crescentus* stalk formation. In *A. biprosthecum*, by contrast, the deletion of *bacA*

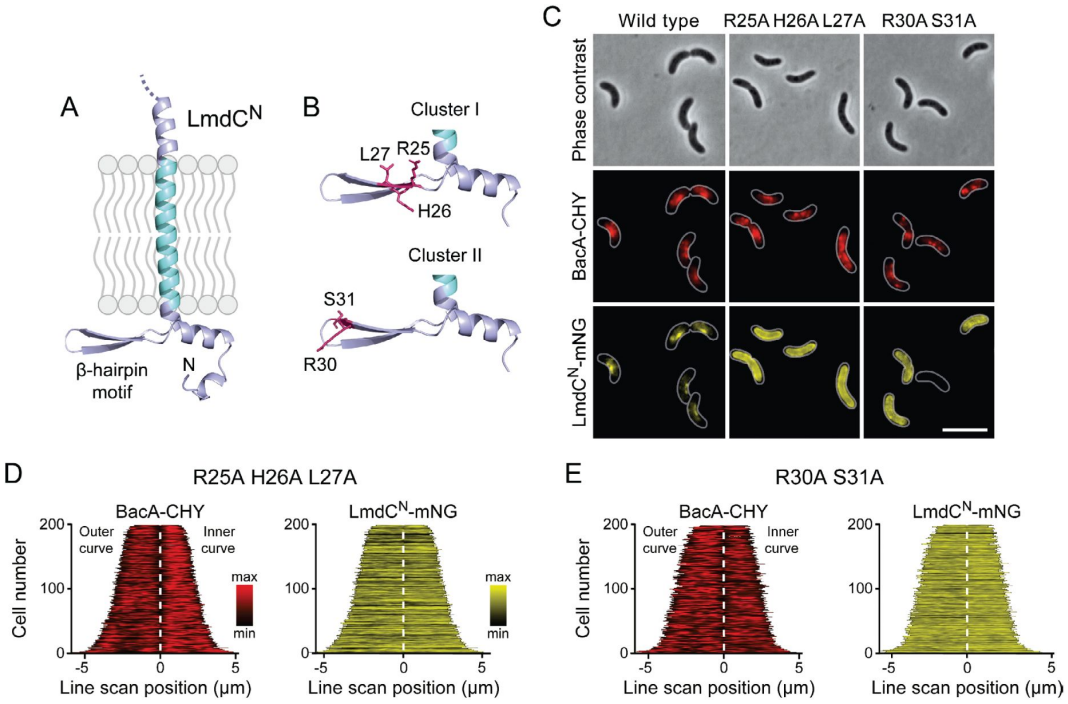

Figure 11.

The β-hairpin in the cytoplasmic region of LmdC is critical for BacA binding.

(A) Predicted structure of LmdC^{N}, comprising the first 80 amino acids of LmdC. The transmembrane domain is colored light blue. The cytoplasmic domain includes a conserved β-hairpin motif. **(B)** Clusters of amino acids mutated for the analysis of BacA-LmdC interaction. Mutated amino acids are shown as red sticks. **(C)** Localization of BacA*Rs*-CHY and the indicated LmdC^{N}*Rs*-mNG variants in the Δ*lmdCRs* background. The Pearson's Correlation Coefficient (PCC) of the two fluorescence signals in a random subpopulation of cells is 0.914 for the wild type fusion (SP119), 0.887 for the R25A-H26A-L27A variant (SP237) and 0.827 for the R30A S31A variant (SP238). Scale bar: 5 μm. **(D,E)** Demographs showing the distribution of BacA-mCherry and (D) R25A-H26A-L27A variant (SP237) or R31A-S31A variant (SP238) of LmdC^{N}-mNG along the outer and inner curve of the cell (n=200 per strain). The white line marks the point of transition from the outer and the inner curve. The analysis was performed as described in **Figure 10F**.

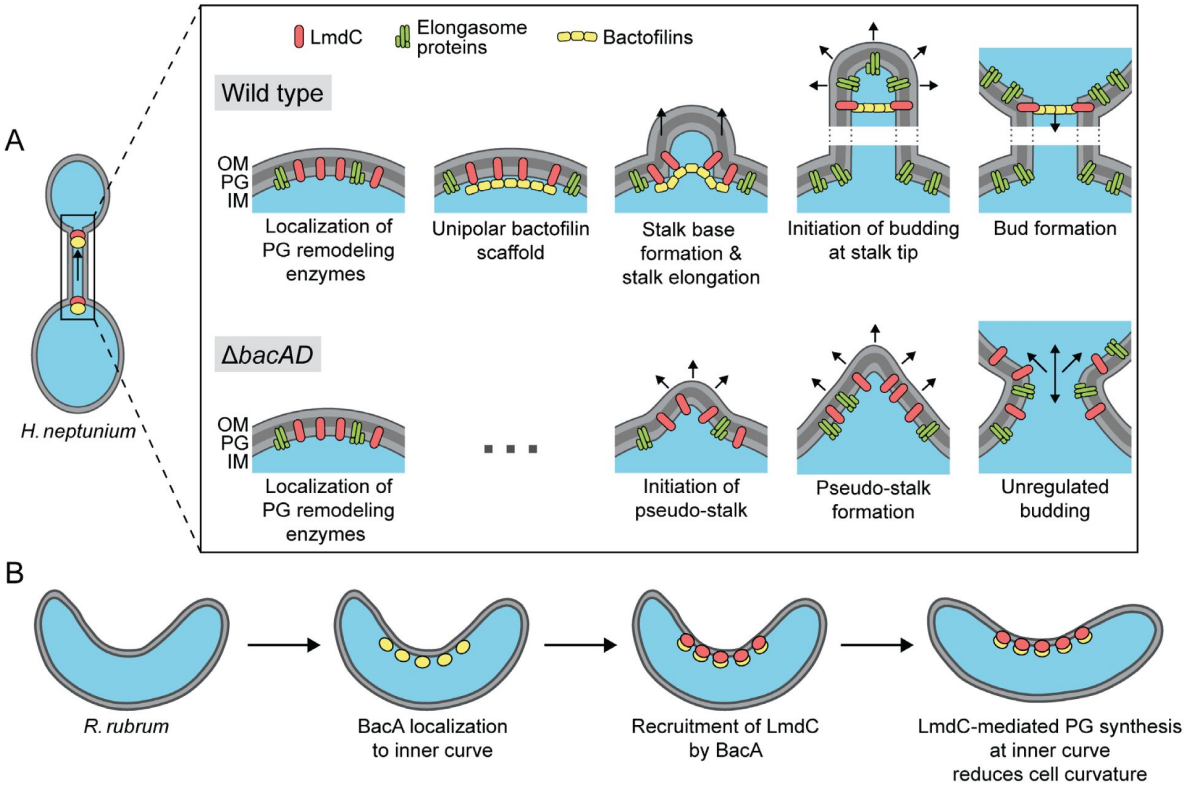

Figure 12.

Model of the roles of BacA and LmdC in *H. neptunium* and *R. rubrum* cell morphogenesis.

(A) Cell morphogenesis in *H. neptunium* wild-type (top) and Δ*bacAD* cells (bottom). In wild-type cells, BacA polymers form a complex with the DD-endopeptidase LmdC at the future stalked pole. The hydrolytic activity of LmdC, possibly stimulated by its interaction with BacA, helps to curve the cell wall at the incipient stalk base and thus determine stalk morphology. The zone of high positive inner cell curvature and, potentially, the physical barrier constituted by the bactofilin polymer prevent the movement of elongasome complexes from the mother cell body into the stalk, thereby limiting peptidoglycan biosynthesis to the stalked cell pole. At a later stage, the bactofilin-LmdC complex localizes close to the tip of the stalk and again generates a ring-shaped zone of positive cell curvature, thereby promoting the remodeling of the stalk tip into a spherical bud. At the onset of the budding process, elongasome complexes accumulate in the nascent bud by a so-far unknown mechanism. The positively curved bud neck and the bactofilin polymers prevent the movement of elongasome complexes from the bud into the stalk, thereby limiting cell growth to the bud compartment. In the Δ*bacAD* mutant, cells fail to concentrate LmdC at the future stalk base and bud neck. As a consequence, peptidoglycan biosynthesis is no longer limited to the different growth zones, leading to pseudo-stalk formation and unregulated bud expansion. **(B)** Bactofilin-mediated modulation of cell helicity in *R. rubrum*. BacA*Rs* (yellow) recruits LmdC*Rs* (red) to the inner cell curvature. The hydrolytic activity of LmdC ultimately stimulates peptidoglycan biosynthesis at this position, leading to a reduction in cell helicity.

completely abolishes stalk formation in rich medium and leads to the formation of wide cellular protrusions, named pseudostalks, under phosphate-limiting conditions (Caccamo et al., 2020). Similar to the amorphous extensions observed for the *H. neptunium* Δ*bacAD* mutant, these structures grow through disperse incorporation of new peptidoglycan and develop into viable offspring. Their formation was also attributed to the entry of cell wall biosynthetic proteins into nascent stalks (Caccamo et al., 2020), suggesting that the *H. neptunium* and *A. biprosthecum* BacA homologs share the same barrier function during stalk formation. However, in *H. neptunium*, another layer of regulation has been added in which bactofilins establish a second barrier close to the stalk tip that enables the formation of stalk-terminal buds. Bud expansion requires the relocation of elongasome complexes from the mother cell to the nascent bud at the onset of bud formation, as likely reflected by the fact that components of the elongasome (MreB, RodZ) and new cell wall biosynthesis can be detected within the stalk during a short time window at the end of the stalk elongation phase (Cserti et al., 2017). This process may be facilitated by the (partial) disassembly of the bactofilin complex at the stalk base and the diffusion of its components to the bud compartment, but the mechanistic details remain to be investigated. Another open question concerns the factors that control the dynamic localization of bactofilin to the stalked pole and the future bud neck in the terminal segment of the stalk. In *A. biprosthecum*, the recruitment of BacA assemblies to the sites of stalk biosynthesis is dependent on the cell wall hydrolase SpmX (Caccamo et al., 2020). However, an *H. neptunium* mutant lacking this protein shows normal morphology (Leicht et al., 2020), suggesting the existence of a different localization determinant.

Intriguingly, bactofilins not only mediate stalk formation and stalk-terminal budding but also the formation of curved cell shapes. We show that both BacA and LmdC are required to establish the normal degree of cell helicity in *R. rubrum*, with their absence leading to hyper-curved cells (**Figure 10C,D**). This result suggests that the two proteins form an accessory module that counteracts the activity of a so-far unknown system responsible for generating spiral cell shape in *R. rubrum* (**Figure 12B**). Cell curvature was shown to promote cell motility (Martinez et al., 2016). It is tempting to speculate that the expression of *bacA* and *lmdC* could be controlled in response to external cues to ensure optimal cell helicity and, thus, fitness in different environments. Our results show that *R. rubrum* cells contain multiple BacA-LmdC complexes that are distributed along the entire cell envelope but localize preferentially to the inner cell curvature (**Figure 10E,G**). In this system, it is immediately obvious that BacA acts as a localization determinant for LmdC, since the preferential localization of LmdC to the inner curve is abolished in its absence (**Figure 10I,J**). To reduce cell curvature, the hydrolytic activity of LmdC must ultimately stimulate the insertion of new peptidoglycan at the inner curve of the cell, which increases the rate of cell elongation in this region and thus straightens the cell body. A similar mechanism may also be at work in the spirochete *L. biflexa*, where the loss of the bactofilin paralog LbbD, whose gene lies adjacent to a gene for putative M23 peptidase (LEPBI_I1430) (**Figure 7A**), was found to induce a strong increase in cell helicity (Jackson et al., 2018). A different variation of this theme is found in *H. pylori*. There, the bactofilin homolog CcmA also forms multiple assemblies along the cell envelope, which interact with a membrane-spanning protein complex including an M23 peptidase (Csd1) homologous to LmdC (Sichel et al., 2022; Taylor et al., 2020). However, these assemblies are enriched at the outer curve of the cell, where they stimulate peptidoglycan synthesis to locally increase the rate of cell elongation over that at the inner curve, leading to twisting of the cell body.

Notably, in all systems characterized so far in molecular detail, the function of bactofilin-M23 peptidase complexes involves the stimulation of cell wall biosynthesis in a confined region of the cell envelope that entails a local change in cell envelope curvature. In *H. neptunium*, these complexes are only localized to narrow bands at the stalk base and bud neck, generating sharp bends at the transition zones between the stalk and the adjacent mother cell and bud compartments. In spiral-shaped bacteria, by contrast, they are scattered along the entire length of

the cell, thereby establishing an elongated zone of increased longitudinal growth that changes overall cell curvature. The same mechanistic principle may also explain the morphogenetic role of bactofilins in so-far uninvestigated systems.

Collectively, our results underscore the role of bactofilins as versatile modulators of bacterial cell shape. In association with M23 peptidases, they form cell wall biosynthetic complexes that introduce local changes in cell envelope curvature. In doing so, they complement the activities of the tubulin and actin cytoskeletons in cell shape determination and thus expand the morphogenetic potential of bacteria, enabling the generation of complex cell shapes that go beyond the generic rod-like or spherical morphologies. It will be interesting to investigate the molecular function of bactofilins in a range of morphologically diverse species to obtain a comprehensive picture of the functionalities provided by these cytoskeletal proteins and the conservation of their mode of action.

Materials and methods

Media and growth conditions

H. neptunium LE670 (ATCC 15444) (Leifson, 1964) and its derivatives were grown in Artificial Sea Salt (ASS) medium at 28 °C under aerobic conditions, shaking at 210 rpm in baffled flasks. ASS medium was composed of 0.5% Bacto Peptone (Thermo Fisher Scientific, USA), 0.1% yeast extract, 1 mM $MgSO_4$, 0.5 mM $CaCl_2$ and 1.5% Instant Ocean Sea Salt (Spectrum Brands, USA), dissolved in deionized water. For solid media, 1.5% agar was added prior to autoclaving. When appropriate, antibiotics were used at the following concentrations (µg/mL in liquid/solid medium): rifampicin (1/2), kanamycin (100/200). The expression of genes under the control of the copper-inducible P_{Cu} promoter or the zinc-inducible P_{Zn} promoter (Jung et al., 2015) was induced by the addition of $CuSO_4$ or $ZnSO_4$ to the concentrations indicated in the text. To assess the growth of *H. neptunium*, cells were grown to exponential phase, diluted in fresh medium to an optical density at 580 nm (OD_{580}) of 0.02, and transferred into 24-well polystyrene microtiter plates (Becton Dickinson Labware, USA). Growth was then followed at 32 °C under double-orbital shaking in an EPOCH 2 microplate reader (BioTek, USA) by measuring the OD_{580} at 20-min intervals.

R. rubrum S1 (ATCC 11170) (Molisch, 1907; Pfennig and Trüper, 1971; van Niel, 1944) and its derivatives were grown in Bacto Tryptic Soy Broth (BD Diagnostic Systems, USA) at 28 °C under aerobic conditions, shaking at 210 rpm in Erlenmeyer flasks. When appropriate, media were supplemented with antibiotics at the following concentrations (µg/mL in liquid/solid medium): kanamycin (30/30), cefalexin (15/-).

E. coli strains were cultivated aerobically (shaking at 210 rpm) at 37 °C in LB medium. For plasmid-bearing strains, antibiotics were added at the following concentrations (µg/mL in liquid/solid medium): kanamycin (30/50), rifampicin (25/50), ampicillin (50/200). To grow *E. coli* WM3064, media were supplemented with 2,6-diaminopimelic acid (DAP) to a final concentration of 300 µM.

Determination of growth rates

Exponentially growing cultures were diluted to an OD_{580} of ~0.01, transferred to a 96-well plate and incubated at 30°C with double-orbital shaking at 355 cpm in an Epoch 2 microplate reader (BioTek, Germany). Growth was monitored by measuring the OD_{600} at 10-min intervals until the stationary phase was reached. OD_{600} measurements obtained in the exponential phase were used to calculate the growth rate μ (increase in OD_{600} per hour). The doubling time t_d was then calculated using the equation $t_d=\ln(2)/\mu$.

Plasmid and strain construction

The bacterial strains, plasmids, and oligonucleotides used in this study are listed in **Supplementary file 1**. *E. coli* TOP10 (Thermo Fisher Scientific, USA) was used as host for cloning purposes. All plasmids were verified by DNA sequencing. *H. neptunium* and *R. rubrum* were transformed by conjugation using the DAP-auxotrophic strain *E. coli* WM3064 as a donor (Jung et al., 2015). The integration of non-replicating plasmids at the chromosomal P_{Cu} or P_{Zn} locus of *H. neptunium* was achieved by single homologous recombination (Jung et al., 2015). Gene replacement in *H. neptunium* and *R. rubrum* was achieved by double-homologous recombination using the counter-selectable *sacB* marker (Cserti et al., 2017). Proper chromosomal integration or gene replacement was verified by colony PCR.

Live-cell imaging

Cells of *H. neptunium* and *R. rubrum* were grown to exponential phase in the appropriate medium and, if suitable, induced with $CuSO_4$ prior to imaging. For depletion experiments, cells were grown in the presence of inducer, washed three times with inducer-free medium and then further cultivated in the absence of inducer for the indicated period of time prior to analysis. To acquire still images, cells were transferred onto 1% agarose pads (in water). For time-lapse analysis, cells were immobilized on pads made of 1% agarose in ASS medium, and the cover slides were then sealed with VLAP (1:1:1 mixture of vaseline, lanolin, and paraffin) to prevent dehydration. Imaging was performed using a Zeiss Axio Imager.M1 microscope equipped with a Zeiss alpha Plan-Apochromat 100x/1.40 Oil DIC objective and a pco.edge 3.1 sCMOS camera (PCO, Germany) or a Zeiss Axio Imager.Z1 microscope equipped with a Zeiss alpha Plan-Apochromat 100x/1.46 Oil DIC M27 or a Plan-Apochromat 100x/1.40 Oil Ph3 M27 objective and a pco.edge 4.2 sCMOS camera (PCO, Germany). An X-Cite 120PC metal halide light source (EXFO, Canada) and ET-DAPI, ET-YFP or ET-TexasRed filter cubes (Chroma, USA) were used for fluorescence detection. Microfluidic experiments were performed using a CellASIC ONIX EV262 Microfluidic System, equipped with an F84 manifold and B04A microfluidic plates (Merck Millipore, Germany), which were flushed with PBS buffer for 30 min before usage. Exponentially growing cells were flushed into the flow cells, cultivated under continuous medium flow (0.4 ml/h), and imaged at regular intervals using the Axio Image.Z1 microscope described above. To visualize sites of ongoing peptidoglycan synthesis, cells were grown to the exponential phase, incubated for 1 min with 1 mM HADA and washed four times in ASS medium prior to imaging.

Images were recorded with VisiView 3.3.0.6 (Visitron Systems, Germany) and processed with ImageJ (Schneider et al., 2012) and Adobe Illustrator CS6 (Adobe Systems, USA). The subcellular distribution of fluorescence signals was analyzed with BacStalk (Hartmann et al., 2020). Pearson's correlation coefficients were determined using the JACoP plug-in (Bolte and Cordelieres, 2006) for ImageJ. Cell sinuosity was determined using the ImageJ plug-in MicrobeJ (Ducret et al., 2016), with each analysis performed in triplicate and 100 cells analyzed per strain and experiment. Results were displayed as SuperPlots (Lord et al., 2020) generated using the SuperPlotsOfData web application (Goedhart, 2021).

To analyze the distribution of fluorescently tagged BacA and LmdC variants along the outline of *R. rubrum* cells, the fluorescence intensity along the outer and inner curve was determined for 200 cells per strain using Fiji (Schindelin et al., 2012). After concatenation of the two fluorescence profiles obtained for each cell, the combined profiles were plotted as demographs, using R 4.2.3 (R Development Core Team, 2012) and the Cell-Profiles package (github.com/ta-cameron/Cell-Profiles/wiki/Vignette) (Cameron et al., 2014).

Single-particle tracking and diffusion analysis

Cells were cultivated overnight in ASS medium, transferred into fresh medium and grown to exponential phase prior to imaging by slimfield microscopy (Plank et al., 2009). In this approach, the back aperture of the objective is underfilled by illumination with a collimated laser beam of

reduced width, generating an area of ~10 µm in diameter with a light intensity high enough to enable the visualization of single fluorescent protein molecules at very high acquisition rates. The single-molecule level was reached by bleaching of most molecules in the cell for 100 to 1,000 frames, followed by tracking of the remaining and newly synthesized molecules for ~3,000 frames. Images were taken at 30 ms intervals using an Olympus IX-71 microscope equipped with a UAPON 100x/ NA 1.49 TIRF objective, a back-illuminated electronmultiplying charge-coupled device (EMCCD) iXon Ultra camera (Andor Solis, USA) in stream acquisition mode, and a LuxX 457-100 (457 nm, 100 mW) light-emitting diode laser (Omicron-Laserage Laserprodukte GmbH, Germany) as an excitation light source. The laser beam was focused onto the back focal plane and operated during image acquisition with up to 2 mW (60 W/cm^2 at the image plane). Andor Solis 4.21 software was used for camera control and stream acquisition. Prior to analysis, frames recorded before reaching the single-molecule level were removed from the streams, using photobleaching curves as a reference. Subsequently, the streams were cropped to an equal length of 2,000 frames and the proper pixel size (100 nm) and time increment were set in the imaging metadata using Fiji (Schindelin et al., 2012). Single particles were tracked with u-track 2.2 (Jaqaman et al., 2008). Trajectories were only considered for further statistical analysis if they had a length of at least five steps. Data analysis was performed using SMTracker 2.0 (Oviedo-Bocanegra et al., 2021). An estimate of the diffusion coefficient and insight into the kind of diffusive motion exhibited were obtained from mean-squared-displacement (MSD)-versus-time-lag curves. In addition, the frame-to-frame displacements of all molecules in x and the y direction were fitted to a two-population Gaussian mixture model to determine the proportions of mobile and static molecules in each condition (Oviedo-Bocanegra et al., 2021).

Transmission electron microscopy

Images of *H. neptunium* cells, 10 µl of early exponential cell cultures were applied onto glow-discharged electron microscopy grids (Formvar/Carbon Film on 300 Mesh Copper; Plano GmbH, Germany) and incubated for 1 min at room temperature. The grid was manually blotted with Whatman filter paper to remove excess liquid. Subsequently, the cells were negatively stained for 5 sec with 5 µl of 1% uranyl acetate. After three washes with H_2O, the grids were dried and imaged in a 100 kV JEM-1400 Plus transmission electron microscope (JEOL, USA). To image BacA polymers, purified BacA-His_6 was dialyzed against low-salt buffer (50 mM HEPES pH 7.2, 10 mM NaCl, 5 mM $MgCl_2$, 0.1 mM EDTA, 1 mM ß-mercaptoethanol) for 16 h. The protein was spotted onto carbon-coated grids and allowed to settle for 2 min. The grids were blotted dry, stained with 1:2 diluted supernatant of saturated 2 % uranyl acetate (in H_2O) for 1 min, dried and imaged using a Zeiss CEM902 electron microscope, operated at 80 kV and equipped with a 2048x2048 pixel CCD camera. Image processing was carried out using Photoshop CS2 and Illustrator CS5 (Adobe Systems, USA).

Immunoblot analysis

Antibodies against BacA were raised by immunization of rabbits with purified BacA-His_6 protein (Eurogentec, Belgium). Cells were harvested in the exponential growth phase. Immunoblot analysis was conducted as described previously (Thanbichler and Shapiro, 2006), using anti-BacA antiserum (1:10.000), a monoclonal anti-mNeonGreen antibody (Chromotek, Germany; Cat. #: 32f6; RRID: AB_2827566), a polyclonal anti-GFP antibody (Sigma, Germany; Cat. #: G1544; RRID: AB_439690), a polyclonal anti-mCherry antibody (BioVision, USA; Cat. #: 5993; RRID: AB_1975001) or a monoclonal anti-HA antibody (Merck Millipore, USA; Cat. #: 05-904; RRID: AB_11213751) at dilutions of 1:10,000, 1:1,000, 1:10,000, 1:10,000 or 1:1,000, respectively. Goat anti-rabbit immunoglobulin G conjugated with horse-radish peroxidase (Perkin Elmer, USA) or goat anti-mouse immunoglobulin G conjugated with horse-radish peroxidase (Sigma, Germany) were used as secondary antibodies. Immunocomplexes were detected with the Western Lightning Plus-ECL chemiluminescence reagent (Perkin Elmer, USA). The signals were recorded with a ChemiDoc MP imaging system (BioRad, Germany) and analyzed using Image Lab software (BioRad, Germany).

Peptidoglycan analysis

Cultures of exponentially growing cells of the *H. neptunium* wild type and its mutant derivatives EC28 (Δ*bacA*), EC23 (Δ*bacD*) and EC33 (Δ*bacAD*) were rapidly cooled to 4°C and harvested by centrifugation at 16,000 ×g for 30 min. The cells were resuspended in 6 ml of ice-cold H_2O and added dropwise to 6 ml of a boiling solution of 8% sodium dodecylsulfate (SDS) that was stirred vigorously. After 30 min of boiling, the suspension was cooled to room temperature. Peptidoglycan was isolated from the cell lysates as described previously (Glauner, 1988) and digested with the muramidase cellosyl (kindly provided by Hoechst, Frankfurt, Germany). The resulting muropeptides were reduced with sodium borohydride and separated by HPLC following an established protocol (Bui et al., 2009; Glauner, 1988). The identity of eluted fragments was assigned based on the known retention times of muropeptides, as reported previously (Cserti et al., 2017; Glauner, 1988).

Protein purification

To purify BacA-His_6, *E. coli* Rosetta(DE3)pLysS (Invitrogen) was transformed with pEC86 and grown in LB medium at 37 °C to an OD_{600} of 0.8. Isopropyl-β-D-1-thiogalactopyranoside (IPTG) was added to a final concentration of 0.5 mM and the incubation was continued for another 3 h. The cells were harvested by centrifugation for 15 min at 7,500 ×g and 4 °C and washed with buffer B2 (50 mM NaH_2PO_4, 300 mM NaCl, 10 mM imidazole, adjusted to pH 8.0 with NaOH). Subsequently, they were resuspended in buffer B2 containing 100 µg/mL phenylmethylsulfonyl fluoride, 10 µg/mL DNase I and 1 mM β-mercaptoethanol and lysed by three passages through a French press at 16,000 psi. After the removal of cell debris by centrifugation at 30,000 ×g for 30 min, the supernatant was applied onto a 5 mL HisTrap HP column (GE Healthcare) equilibrated with buffer B3 (50 mM NaH_2PO_4, 300 mM NaCl, 20 mM imidazole, adjusted to pH 8.0 with NaOH). The column was washed with 10 column volumes (CV) of the same buffer, and protein was eluted at a flow rate of 1 mL/min with a linear imidazole gradient obtained by mixing buffers B3 and B4 (50 mM NaH_2PO_4, 300 mM NaCl, 250 mM imidazole, adjusted to pH 8.0 with NaOH). Fractions containing high concentrations of BacA-His_6 were pooled and dialyzed against 3 L of buffer B5 (20 mM Tris/HCl pH 8.0, 10 mM NaCl, 1 mM β-mercaptoethanol) at 4 °C. After the removal of precipitates by centrifugation at 30,000 ×g for 30 min, the protein solution was aliquoted and snap-frozen in liquid nitrogen. Aliquots were stored at -80 °C until further use.

To purify LmdC, the protein was first produced as a His_6-SUMO-LmdC fusion (Marblestone et al., 2006). To this end, *E. coli* Rosetta(DE3)pLysS cells carrying plasmid pLY015 were grown at 37 °C in 3 L of LB medium supplemented with ampicillin and chloramphenicol. At an OD_{600} of 0.6, the culture was chilled to 18°C, and protein synthesis was induced by the addition of 1 mM IPTG prior to overnight incubation at 18 °C. The cultures were harvested by centrifugation at 10,000 ×g for 20 min at 4 °C and washed with lysis buffer (50 mM Tris/HCl pH 8.0, 300 mM NaCl). Cells were resuspended in lysis buffer supplemented with 5 mM imidazole, 10 mg/mL DNase I and 100 mg/mL PMSF. After three passages through a French press (16,000 psi), the cell lysate was clarified by centrifugation (30,000 ×g, 30 min, 4 °C). Protein was then purified using zinc-affinity chromatography using a 1 mL Zn-NTA column (Cube Biotech) equilibrated with lysis buffer containing 5 mM imidazole. Protein was eluted with a linear gradient of 5 to 250 mM imidazole in lysis buffer at a flow rate of 1 mL/min. Fractions containing high concentrations of His_6-SUMO-LmdC were pooled and dialyzed against 3 L of low-salt lysis buffer (20 mM Tris/HCl pH 7.6, 50 mM NaCl, 10% (v/v) glycerol). After the addition of Ulp1 protease (Marblestone et al., 2006) and dithiothreitol (1 mM), the protein was incubated for 4 h at 4 °C to cleave off the His_6-SUMO tag. The solution was centrifuged for 30 min at 38,000 ×g and 4 °C to remove precipitates and then subjected to ion exchange chromatography using a 1 mL HiTrap Q HP column (Cytiva, USA) equilibrated with low-salt lysis buffer. His_6-SUMO passed the column in the flow-through, and LmdC was eluted with a linear gradient of 150-1000 mM NaCl in low-salt buffer. Fractions containing LmdC were concentrated in an Amicon Ultra-4 10K spin concentrator (MWCO 10,000; Merck, Germany). After the removal of precipitates by centrifugation at 30,000 ×g for 30 min,

LmdC was further purified by size exclusion chromatography (SEC) on a HighLoad 16/60 Superdex 200 pg column (GE Healthcare, USA) equilibrated with SEC buffer (20 mM Tris/HCl pH 7.4, 150 mM NaCl). Fractions containing pure protein were pooled and concentrated. After the removal of precipitates by centrifugation at 30,000 ×g, the protein solution was snap-frozen in liquid N_2 and stored at -80 °C until further use.

LmdC enzymatic activity assay

To test the enzymatic activity of LmdC, peptidoglycan from *E. coli* D456 (Edwards and Donachie, 1993) was mixed with 10 µM LmdC in buffer A (20 mM Hepes/NaOH pH 7.5, 50 mM NaCl, 1 mM $ZnCl_2$) or buffer B (20 mM sodium acetate pH 5.0, 50 mM NaCl, 1 mM $ZnCl_2$) in a final volume of 50 µL and incubated at 37°C for 16 h in a thermal shaker set at 900 rpm. A mixture of peptidoglycan in buffer B without LmdC was used as a control. The reactions were stopped by heating at 100°C for 10 min. The peptidoglycan was then further digested overnight with cellosyl, and the reactions were stopped by heating at 100°C for 10 min. After centrifugation of the samples at 14,000 rpm for 10 min, the supernatants were recovered, reduced with sodium borohydride, acidified to pH 4.0 – pH 4.5 with dilute 20% phosphoric acid and subjected to HPLC analysis as previously described (Glauner, 1988).

Bio-layer interferometry

Bio-layer interferometry analyses were conducted using a BLItz system equipped with High Precision Streptavidin (SAX) Biosensors (Sartorius, Germany). As a ligand, a custom-synthetized N-terminally biotinylated peptide comprising residues Met1 to Gln38 of LmdC (GenScript, USA) was immobilized on the biosensors. After the establishment of a stable baseline, association reactions were monitored at various analyte concentrations. At the end of each binding step, the sensor was transferred into an analyte-free buffer to follow the dissociation kinetics. The extent of non-specific binding was assessed by monitoring the interaction of analyte with unmodified sensors. All analyses were performed in BLItz binding buffer (25 mM HEPES/KOH pH 7.6, 100 mM KCl, 10 mM $MgSO_4$, 1 mM DTT, 10 mM BSA, 0.01% Tween).

Bioinformatic analysis

Protein similarity searches were performed with BLAST (Altschul et al., 1990), using the BLAST server of the National Institutes of Health (*https://blast.ncbi.nlm.nih.gov/Blast.cgi*). Transmembrane helices were predicted with DeepTMHMM (Hallgren et al., 2022), coiled-coil regions with PCOILS (Lupas, 1996). The positions of conserved functional domains were determined using the PFAM server (Mistry et al., 2021). AlphaFold2 (Jumper et al., 2021) and AlphaFold-Multimer (Evans et al., 2022), as implemented in the AlphaFold.ipynb notebook on Google Colab, were used to predict the tertiary or quaternary structure of proteins, respectively. SuperPlots (Lord et al., 2020) were used to visualize cell length distributions and to evaluate the statistical significance of differences between multiple distributions, employing the PlotsOfData web app (Postma and Goedhart, 2019).

Acknowledgements

We thank Julia Rosum for excellent technical assistance, Svenja Urban and Ying Liu for help with the construction of plasmids, Daniela Vollmer for the purification of peptidoglycan, and Maria Perez-Burgos and Lotte Søgaard-Andersen for help with the transmission electron microscopy analyses.

Additional information

Funding

Funder	Grant reference number	Author
University of Marburg	Core funding	Peter L. Graumann Martin Thanbichler
Max Planck Society	Max Planck Fellowship	Martin Thanbichler
German Research Foundation (DFG)	450420164	Martin Thanbichler
German Research Foundation (DFG)	26942323 – TRR 174	Peter L. Graumann
United Kingdom Biotechnology and Biological Sciences Research Council	BB/W013630/1	Waldemar Vollmer
Max Planck Society	PhD fellowship of the International Max Planck Research School for Environmental, Cellular and Molecular Microbiology (IMPRS-Mic)	Manuel Osorio-Valeriano

The funders had no role in the design of the study, the collection and interpretation of the data, or the decision to submit the work for publication.

Author contributions

S.P., M.O.V., E.C. and M.T. conceived the study. S.P., M.O.V., E.C. and J.H. constructed plasmids and strains and performed the growth analyses and subcellular localization studies. M.O.V. purified proteins and conducted the biochemical studies. J.H. established the CRISPRi system for *H. neptunium*. R.H.-T. performed the single-particle tracking analysis. J.B. conducted the peptidoglycan analysis. P.S. analyzed the coconservation of BacA and LmdC homologs. S.P., M.O.V., E.C., R.H.-T., P.S., J.B., W.V. and M.T. analyzed the data. W.V., P.L.G. and M.T. supervised the study. W.V., P.L.G. and M.T. secured funding. S.P., M.O.V. and M.T. wrote the paper, with input from all other authors.

Data availability

All relevant data generated in this study are included in the manuscript and the supplemental information.

Competing interests

The authors declare no competing interests.

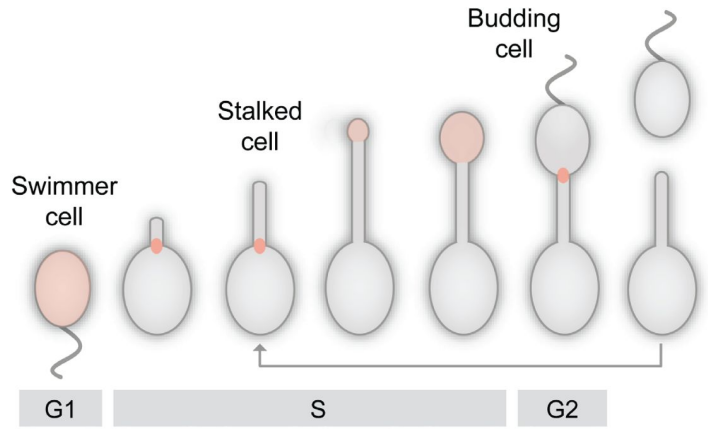

Figure 1—figure supplement 1.

The dimorphic lifecycle of *H. neptunium*.

A motile, flagellated swimmer sheds its flagellum and forms a stalk at the opposite cell pole. At a defined point in the cell cycle, the terminal segment of the stalk dilates and develops into a new swimmer cell. After cell division, the newborn swimmer cell first needs to differentiate into a stalked cell to initiate a new round of cell division, whereas the stalked mother cell immediately enters the next replication cycle. The predominant growth zones (Cserti et al., 2017) are indicated in red.

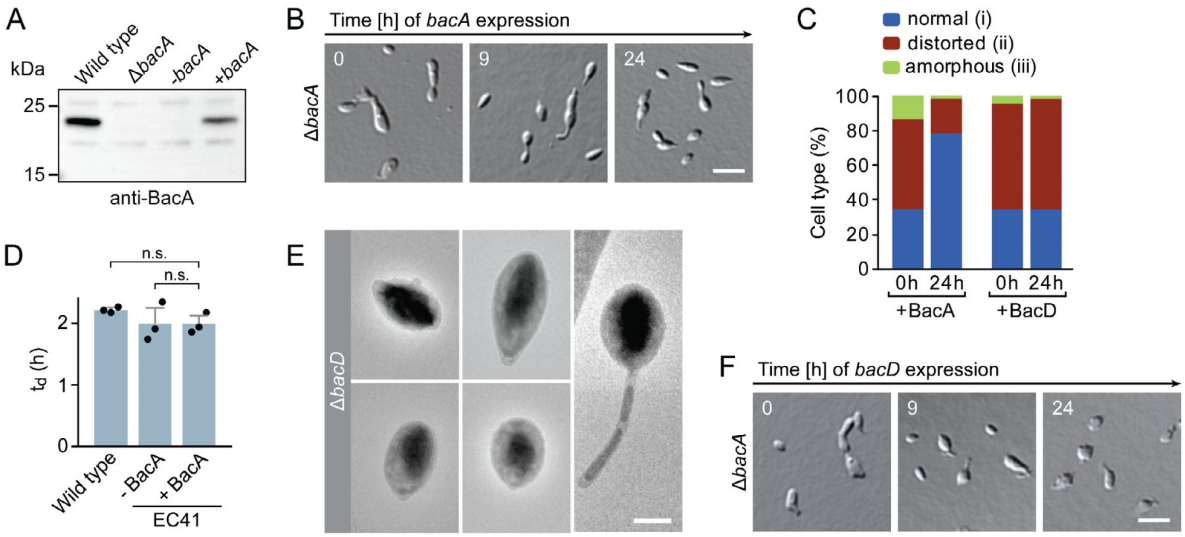

Figure 1—figure supplement 2.

Phenotypic analysis of *H. neptunium* bactofilin mutants.

(A) Immunoblot analysis of strains LE670 (wild type), EC28 (Δ*bacA*) and EC41 (Δ*bacA* PCu::PCu-*bacA*) grown in the absence (-*bacA*) and presence (+*bacA*) of 0.5 mM CuSO4, performed with an anti-BacA antibody. **(B)** Rescue of the phenotype of a Δ*bacA* mutant by ectopic expression of *bacA*. Cells of strain EC41 (Δ*bacA* PCu::PCu-*bacA*) were grown in copper-free medium, induced by the addition of copper, and imaged after the indicated time incubation times. Bar: 3 µm. **(C)** Quantification of the proportion of phenotypically abnormal stalked and budding cells in the cultures of strains EC41 (Δ*bacA* PCu::PCu-*bacA*) and EC43 (Δ*bacA* PZn::PZn-*bacD*) analyzed in panels B and E before (t=0 h) and 24 h after induction (n = 100 cells per time point). **(D)** Doubling times of the indicated *H. neptunium* strains. Strain EC41 (Δ*bacA* PCu::PCu-*bacA*) as analyzed in the absence (-) and presence (+) of copper. Strain LE670 (wild-type) grown in copper-free medium is shown as a control. Bars represent the mean (± SD) of three independent experiments (dots). Statistical significance was determined using Welch's non-paired t-test (n.s., not significant). **(E)** Transmission electron micrographs of Δ*bacD* cells at the swimmer and stalk cell stage. Bar: 1 µm. **(F)** DIC images of a Δ*bacA* mutant overproducing BacD from a zinc-inducible promoter. Cells of strain EC43 (Δ*bacA* PZn::PZn-*bacD*) were grown in inducer-free medium, induced by the addition of 0.5 mM ZnSO4, and imaged after the indicated incubation times. Bar: 3 µm.

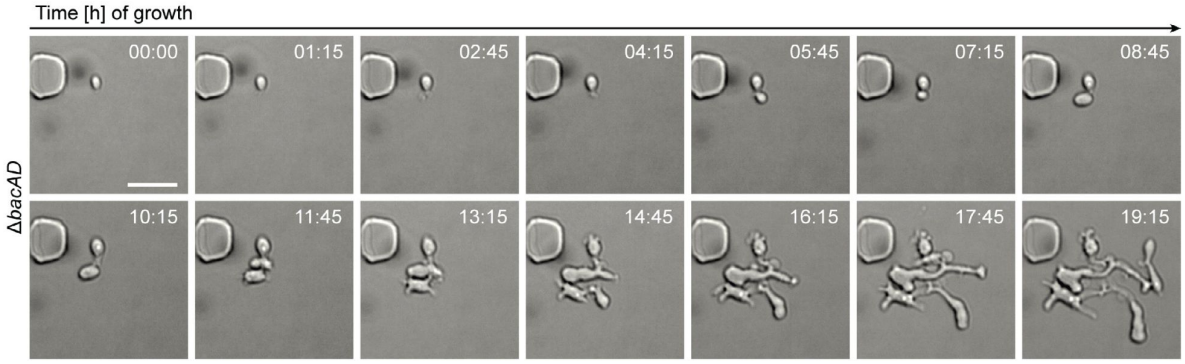

Figure 2—figure supplement 1.

Growth of Δ*bacAD* cells in a microfluidic flow cell.

Cells of strain EC33 (Δ*bacAD*) were flushed into a microfluidic flow cell and imaged at the indicated time points (in h). Bar: 3 µm.

Figure 2—video 1. Unconstrained growth of a bactofilin-deficient *H. neptunium* mutant. Cells of strain EC33 (Δ*badAD*) were grown in a microfluidic flow cell and imaged by DIC microsopy at 15 min intervals. Bar: 2 µm.

Figure 2—video 2. Normal growth of the *H. neptunium* wild-type strain. Cells of strain LE670 (wild type) were grown in a microfluidic flow cell and imaged by DIC microscopy at 5 min intervals. Bar: 2 µm.

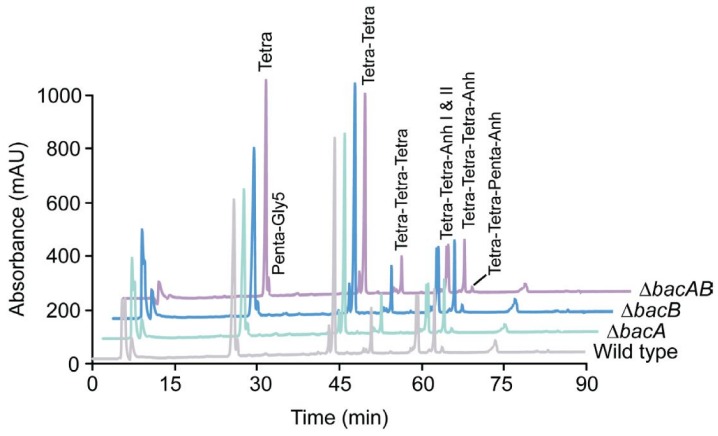

Figure 2—figure supplement 2.

Muropeptide profiles of different *H. neptunium* strains.

Cell walls of strains LE670 (wild type), EC28 (Δ*bacA*), EC23 (Δ*bacD*) and EC33 (Δ*bacAD*) were digested with cellosyl to release muropeptides, which were reduced and separated by HPLC. The identities of major muropeptide species, assigned based on the previously reported retention times (Cserti et al., 2017; Glauner, 1988), are given above the corresponding peaks. Tri, Tetra and Penta stand for N-acetylglucosamine-N-acetylmuramitol tripeptide, tetrapeptide and pentapeptide, respectively. “Anh” indicates muropeptides containing 1,6-anhydromuramic acid.

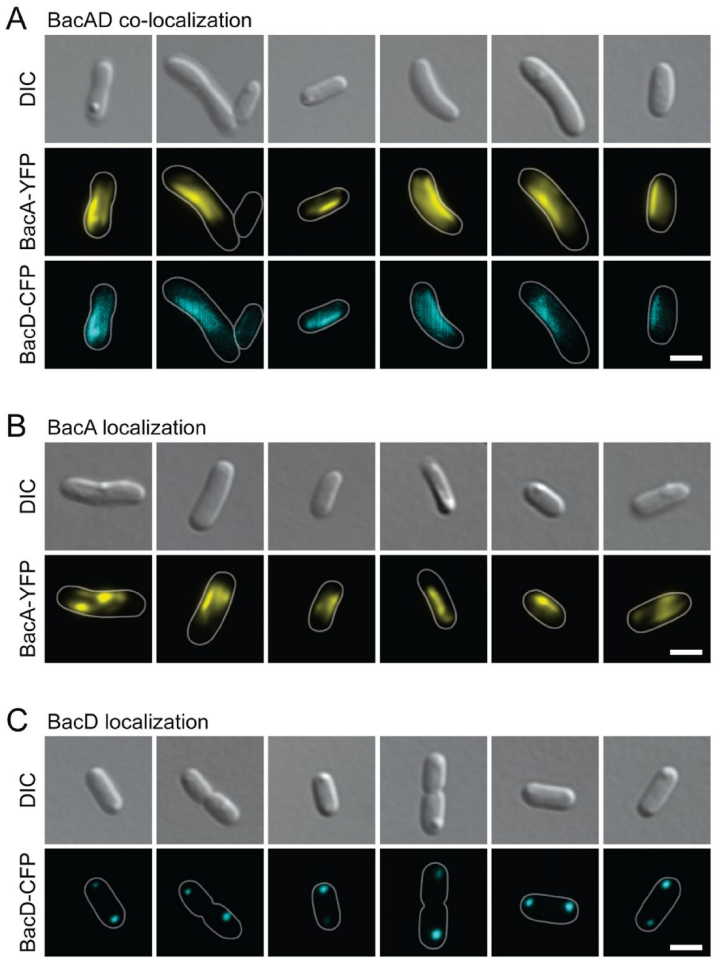

Figure 3—figure supplement 1.

Localization patterns of BacA-YFP and BacD-CFP upon heterologous overproduction in *E. coli*.

(A) Co-localization of BacA-YFP and BacD-CFP in cells of *E. coli* BL21(DE3) transformed with plasmid pEC121 (PT7-*bacA-eyfp* PT7-*bacD-ecfp*). **(B)** Localization of BacA-YFP in cells of *E. coli* BL21(DE3) transformed with plasmid pEC119 (PT7-*bacA-eyf*) **(C)** Localization of BacD-CFP in *E. coli* BL21(DE3) transformed with plasmid pEC120 (PT7-bacD-ecfp). All strains were grown in LB medium containing 5% glucose and induced with 0.5 mM IPTG prior to imaging. Bars: 2 µm.

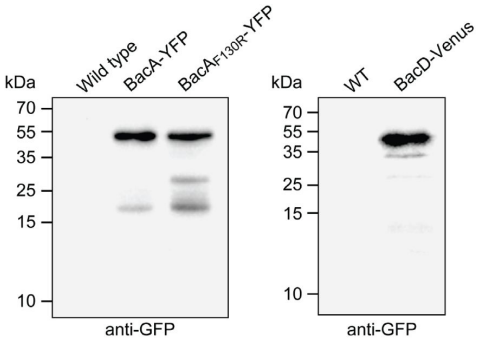

Figure 4—figure supplement 1.

Stability of the fluorescently tagged bactofilin derivatives used in this study.

Cells of strains LE670 (wild type), EC61 (*bacA*::*bacA-eyfp*), MO78 (*bacA*::*bacAF130R-eyfp*) and EC67 (*bacD*::*bacD-venus*) were subjected to immunoblot analysis using anti-GFP antibodies.

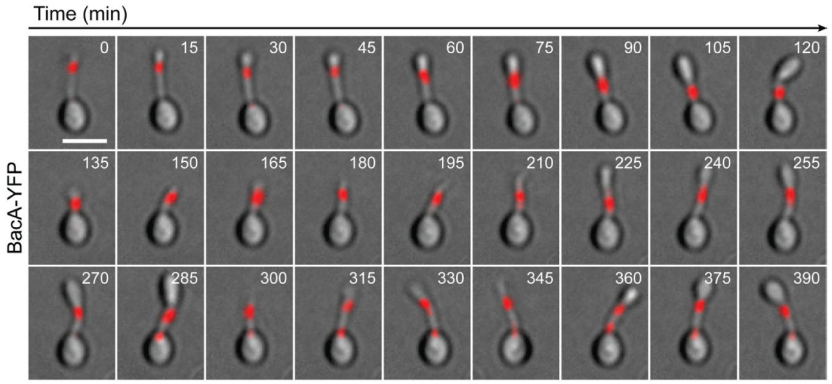

Figure 4—figure supplement 2.

Localization dynamics of BacA-YFP.

Cells of strain EC61 (*bacA*::*bacA-eyfp*) were flushed into a microfluidic flow cell and imaged at 15-min intervals over multiple cell cycles. Shown are overlays of DIC and fluorescence images. Bar: 2 µm.

Figure 4—video 1. Localization dynamics of BacA-YFP (example 1). Cells of strain EC61 (*bacA::bacA-eyfp*) were grown in a microfluidic flow cell and imaged at 15 min intervals. Shown are overlays of DIC and fluorescence images. YFP fluorescence is shown in red for better visibility. Bar: 2 µm.

Figure 4—video 2. Localization dynamics of BacA-YFP (example 2). Cells of strain EC61 (*bacA::bacA-eyfp*) were grown in a microfluidic flow cell and imaged at 15 min intervals. Shown are overlays of DIC and fluorescence images. YFP fluorescence is shown in red for better visibility. Bar: 2 µm.

Figure 4—video 3. Localization dynamics of BacA-YFP (example 3). Cells of strain EC61 (*bacA::bacA-eyfp*) were grown in a microfluidic flow cell and imaged at 15 min intervals. Shown are overlays of DIC and fluorescence images. YFP fluorescence is shown in red for better visibility. Bar: 2 µm.

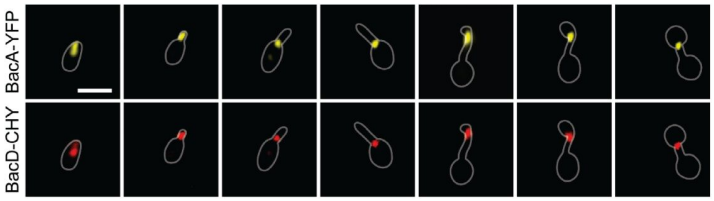

Figure 4—figure supplement 3.

Co-localization of BacA and BacD.

Shown are the individual fluorescence images of strain EC68 (*bac*A::*bacA-eyfp bacD*::*bacD-mCherry*) used to generate the overlays in **Figure 4D**. Bar: 1 µm.

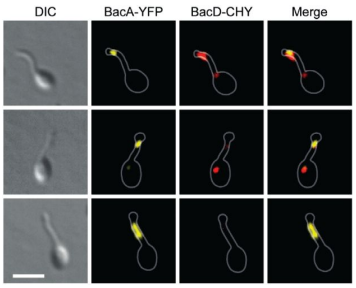

Figure 4—figure supplement 4.

Partial independence of BacA and BacD localization at the onset of the budding process.

Shown are exemplary cells of strain EC68 (*bacA*::*bacA-eyfp bacD*::*bacD-mCherry*) in which BacA-YFP and BacD-CHY do not fully co-localize. Bar: 2 µm.

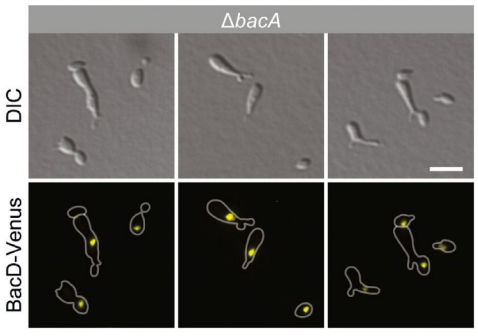

Figure 4—figure supplement 5.

Random localization of BacD complexes in the absence of BacA.

Cells of strain EC60 (Δ*bacA* PZn::PZn-*bacD-venus*) were grown in inducer-free medium and then induced for 4 h with 0.5 mM ZnSO4 prior to imaging. Bar: 3 µm.

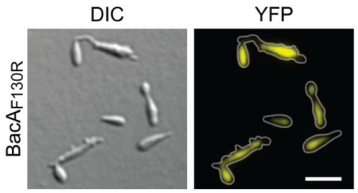

Figure 4—figure supplement 6.

Localization and functionality of BacAF130R-YFP.

Cells of strain MO78 (*bacA*::*bacAF130R-eyfp*), producing the polymerization-deficient BacAF130R-YFP variant instead of the native protein, were grown to exponential phase and imaged. Bar: 3 µm.

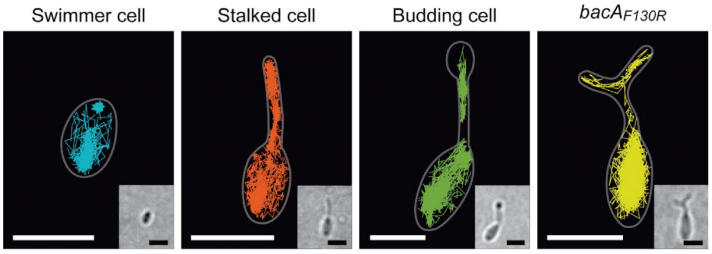

Figure 6—figure supplement 1.

Single-particle tracking analysis of BacA-YFP.

The images show the sums of all single-molecule tracks obtained for individual *H. neptunium* swimmer, stalked and budding cell producing BacA-YFP (EC61) or for a mutant cell producing the polymerization-deficient BacAF130R-YFP variant (MO78). Cell outlines are indicated by white lines. Inserts show the corresponding bright-field images. Bars: 1 µm.

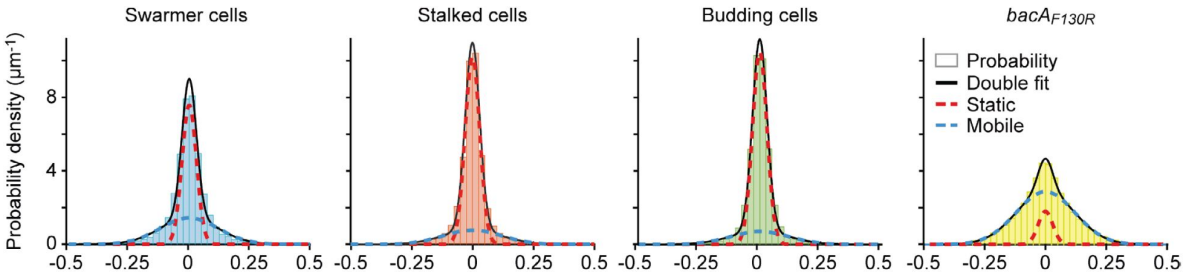

Figure 6—figure supplement 2.

Single-particle tracking analysis of BacA-YFP mobility.

Shown is a Gaussian mixture model (GMM) analysis of the mobility of the BacA-YFP variants plotted in **Figure 5C**. The distributions of the frame-to-frame displacements in both x and y direction from single-particle tracking experiments were fitted to a two-component Gaussian function (sum in black), assuming a fast-diffusing mobile (dotted blue lines) and a slow-diffusing (dotted red lines) population.

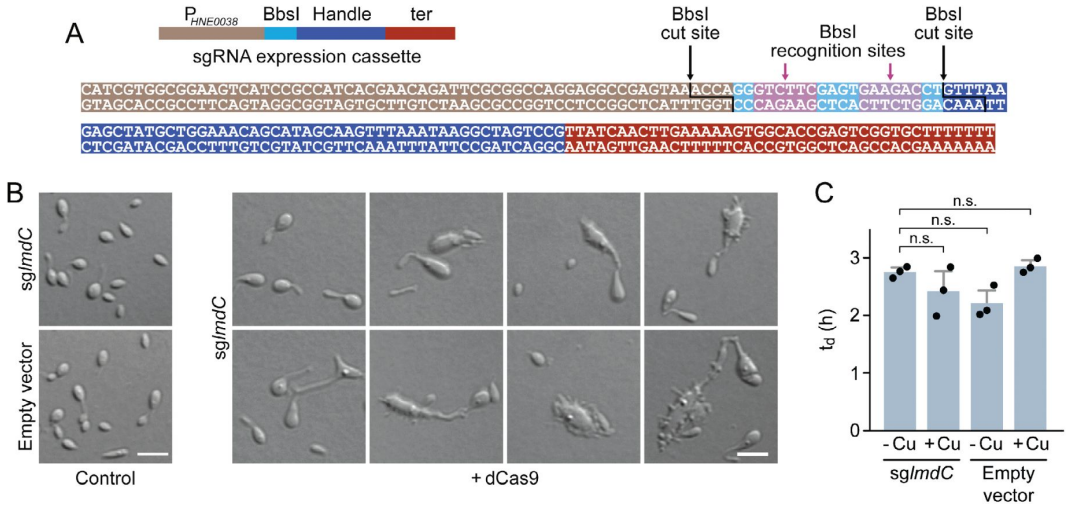

Figure 9—figure supplement 1.

Characterization of the phenotype induced by the CRISPRi-mediated depletion of LmdC in *H. neptunium*.

(**A**) Sequence of the sgRNA expression cassette of pdCas9Entry. The different parts of the sequence are colored as defined in the schematic on top. The BsbI recognition and cut sites are indicated by arrows. **(B)** Morphological diversity of *H. neptunium* cells depleted of LmdC. Shown are representative cells of strains SP236 (*lmdC*::*lmdC*-HA pJH13) (sg*lmdC*) and SP249 (*lmdC*::*lmdC*-HA pCas9Entry) (empty vector) grown for 24 h in the absence (control) or presence (+ dCas9) of 0.3 mM CuSO4. Cells were imaged by DIC microscopy. Bar: 2 µm. **(C)** Doubling times of the strains analyzed in panel B in the absence (-Cu) or presence (+Cu) of 0.3 mM CuSO4. Bars represent the mean (± SD) of three independent experiments (dots). Statistical significance was determined using Welch's non-paired t-test (n.s., not significant).

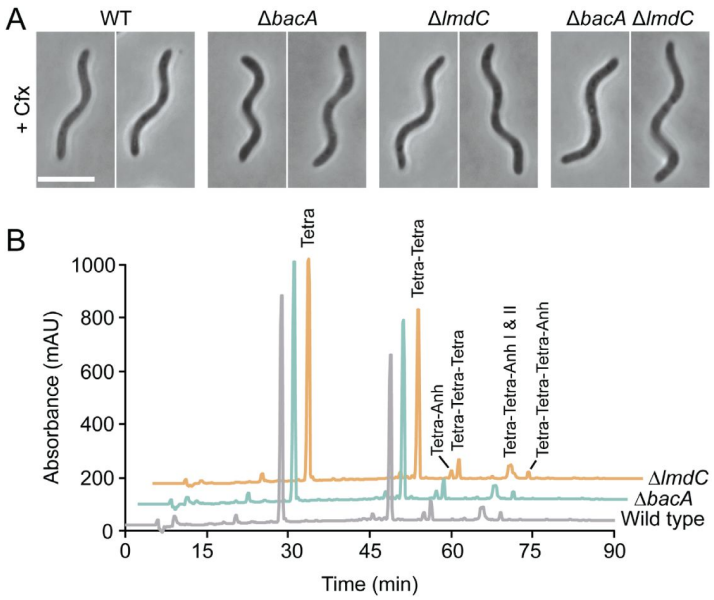

Figure 10—figure supplement 1.

Analysis of BacA and LmdC from *R. rubrum*.

(A) Clearer visualization of the abnormal curvature of BacA- and LmdC-deficient *R. rubrum* cells by inhibition of cell division. Cells of strains SP68 (Δ*lmdC*), SP70 (Δ*bacA*) and SP116 (Δ*lmdC* Δ*bacA*) were treated with 5 µg/ml cefalexin (Cfx) for 6 h. Bar: 5 µm. **(B)** Muropeptide profiles of different *R. rubrum* strains. Cell walls of strains S1 (wild type), SP70 (Δ*bacARs*) and SP68 (Δ*lmdC*) were digested with cellosyl to release muropeptides, which were reduced and separated by HPLC chromatography. The identities of major muropeptide species, assigned based on the previously reported retention times (Glauner, 1988), are given above the corresponding peaks. Tetra stands for N-acetyl-glucosamine-N-acetylmuramitol tetrapeptide. "Anh" indicates muropeptides containing 1,6-anhydromuramic acid.

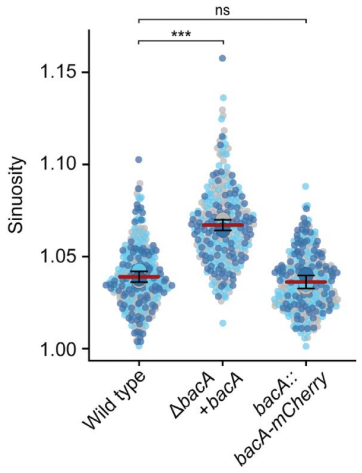

Figure 10—figure supplement 2.

Cell lengths of *R. rubrum* strains.

Superplots showing the distribution of cell sinuosities in populations of strains S1 (wild type), SP105 (Δ*bacARs* P*bacA-bacARs*) and SP109 (*bacARs*::*bacARs-mCherry*). Small dots represent the data points, large dots represent the median values of the three independent experiments shown in the graphs (dark blue, light blue, grey). The mean of the three median values is indicated by a horizontal line. Whiskers represent the standard deviation. *** p<0.005; ns, not significant; t-test).

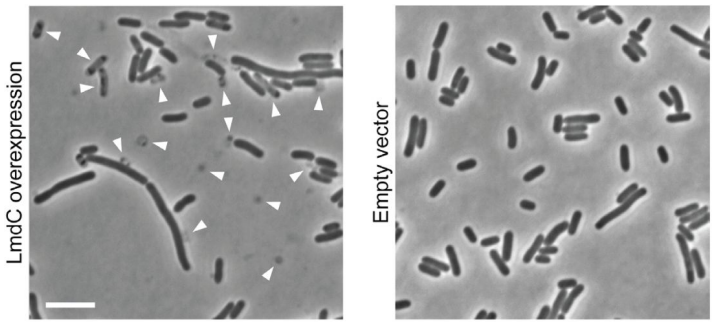

Figure 10—figure supplement 3.

Lysis of *E. coli* upon heterologous expression of full-length *R. rubrum lmdC*.

Shown are cells of *E. coli* Rosetta(DE3)pLysS harboring pSP120 (PT7-*lmdCRs*) or the corresponding empty vector imaged 4h after the induction of gene expression with 0.5 mM IPTG. Arrowheads indicate ghost cells, cell debris, lysing cells or strongly elongated cells. Scale bar: 5 µm.

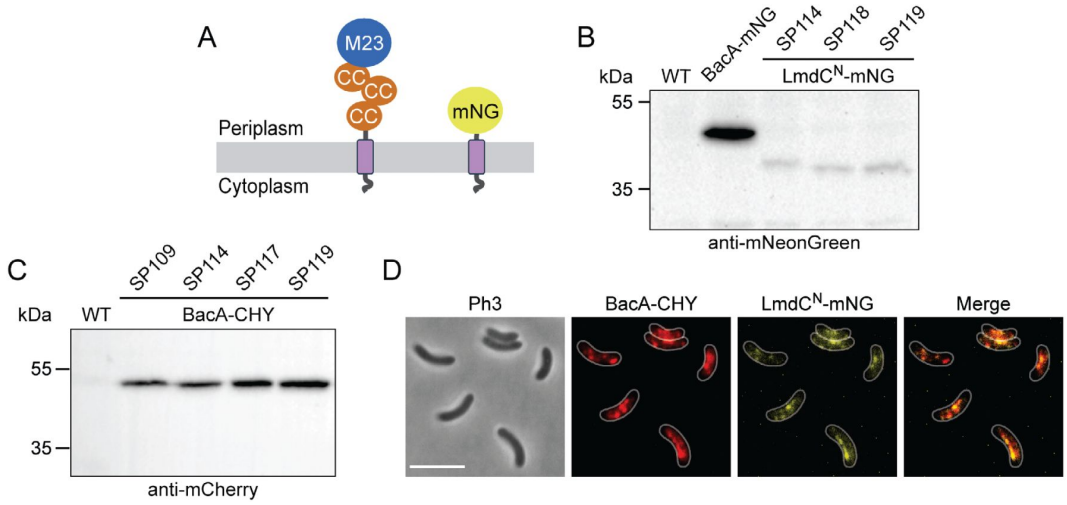

Figure 10—figure supplement 4.

Analysis of *R. rubrum* strains producing fluorescent protein fusions.

(A) Domain architectures of the native LmdC*Rs* protein and the truncated LmdC^{N}*Rs*-mNG reporter construct used for localization studies. The transmembrane helix is shown in purple. Abbreviations: CC (coiled-coil domain), M23 (M23 peptidase domain), mNG (mNeongreen). **(B)** Levels of the LmdC^{N}*Rs*-mNG fusion in different *R. rubrum* strains. Strains SP98 (Δ*lmdCRs bacARs*::*bacARs-mNeongreen*), SP114 (*bacARs*::*bacARs-mCherry* P*lmdC-lmdC*^{N}*Rs-mNeongreen*), SP118 (Δ*bacA* Δ*lmdC* P*lmdC-lmdC1-80-mNeongreen*) and SP119 (*bacA*::*bacA-mCherry* Δ*lmdC* P*lmdC-lmdC1-80-mNeongreen*) were subjected to immunoblot analysis with an anti-mNeonGreen antibody. Predicted molecular weights: BacA*Rs*-mNG (44.8 kDa), LmdC^{N}*Rs*-mNG fusion (35.9 kDa) **(C)** Levels of the BacA*Rs*-CHY fusion in different *R. rubrum* strains. Strains SP109 (*bacARs*::*bacARs-mCherry*), SP114 (*bacARs*::*bacARs-mCherry* P*lmdC-lmdC*^{N}*Rs-mNeongreen*), SP117 (*bacARs*::*bacARs-mCherry* Δ*lmdC*) and SP119 (*bacARs*::*bacARs-mCherry* Δ*lmdC* P*lmdC-lmdC*^{N}*Rs-mNeongreen*) were subjected to immunoblot analysis with an anti-mCherry antibody. The predicted molecular weight of BacA*Rs*-CHY is 44.9 kDa. **(D)** Co-localization of BacA*Rs*-CHY and LmdC*Rs*-mNG in *R. rubrum* cells carrying the native *lmdCRs* gene. The Pearson's Correlation Coefficient (PCC) of the two fluorescence signals in a random subpopulation of cells (n=177) is 0.54. Scale bar: 5 µm.

References

Aaron M, Charbon G, Lam H, Schwarz H, Vollmer W, Jacobs-Wagner C (2007) **The tubulin homologue FtsZ contributes to cell elongation by guiding cell wall precursor synthesis in Caulobacter crescentus** *Molecular Microbiology* **64**:938–952

Altschul SF, Gish W, Miller W, Myers EW, Lipman DJ (1990) **Basic local alignment search tool** *Journal of Molecular Biology* **215**:403–410

Alyahya SA, Alexander R, Costa T, Ao Henriques, Emonet T, Jacobs-Wagner C (2009) **RodZ, a component of the bacterial core morphogenetic apparatus** *Proceedings of the National Academy of Sciences U S A* **106**:1239–1244

Badger JH *et al.* (2006) **Comparative genomic evidence for a close relationship between the dimorphic prosthecate bacteria Hyphomonas neptunium and Caulobacter crescentus** *Journal of Bacteriology* **188**:6841–6850

Bendezú FO, Hale CA, Bernhardt TG, de Boer PAJ. (2009) **RodZ (YfgA) is required for proper assembly of the MreB actin cytoskeleton and cell shape in E. coli** *EMBO Journal* **28**:193–204

Bolte S, Cordelieres FP (2006) **A guided tour into subcellular colocalization analysis in light microscopy** *Journal of Microscopy* **224**:213–232

Brown PJ, Kysela DT, Brun YV (2011) **Polarity and the diversity of growth mechanisms in bacteria** *Seminars in Cell & Developmental Biology* **22**:790–798

Bui NK, Gray J, Schwarz H, Schumann P, Blanot D, Vollmer W (2009) **The peptidoglycan sacculus of Myxococcus xanthus has unusual structural features and is degraded during glycerol-induced myxospore development** *Journal of Bacteriology* **191**:494–505

Caccamo PD, Jacq M, VanNieuwenhze MS, Brun YV (2020) **A division of labor in the recruitment and topological organization of a bacterial morphogenic complex** *Current Biology* **30**:3908–3922

Cameron TA, Anderson-Furgeson J, Zupan JR, Zik JJ, Zambryski PC (2014) **Peptidoglycan synthesis machinery in Agrobacterium tumefaciens during unipolar growth and cell division** *MBio* **5**:e01219–14

Chen B *et al.* (2013) **Dynamic imaging of genomic loci in living human cells by an optimized CRISPR/Cas system** *Cell* **155**:1479–1491

Cserti E, Rosskopf S, Chang YW, Eisheuer S, Selter L, Shi J, Regh C, Koert U, Jensen GJ, Thanbichler M (2017) **Dynamics of the peptidoglycan biosynthetic machinery in the stalked budding bacterium Hyphomonas neptunium** *Molecular Microbiology* **103**:875–895

Deng X, Gonzalez Llamazares A, Wagstaff JM, Hale VL, Cannone G, McLaughlin SH, Kureisaite-Ciziene D, Löwe J (2019) **The structure of bactofilin filaments reveals their mode of membrane binding and lack of polarity** *Nature Microbiology* **4**:2357–2368

Ducret A, Quardokus EM, Brun YV (2016) **MicrobeJ, a tool for high throughput bacterial cell detection and quantitative analysis** *Nature Microbiology* **1**

Edwards D, Donachie WD (1993) **Construction of a triple deletion of penicillin-binding proteins 4, 5, and 6 in Escherichia coli. In: Bacterial growth and lysis, eds: de Pedro M, Höltje J-V** :369–374

Egan AJF, Errington J, Vollmer W (2020) **Regulation of peptidoglycan synthesis and remodelling** *Nature Reviews Microbiology* **18**:446–460

Evans R *et al.* (2022) **Protein complex prediction with AlphaFold-Multimer** *bioRxiv* https://doi.org/10.1101/2021.1110.1104.463034

Figueroa-Cuilan WM, Randich AM, Dunn CM, Santiago-Collazo G, Yowell A, Brown PJB (2021) **Diversification of LytM protein functions in polar elongation and cell division of Agrobacterium tumefaciens** *Frontiers in Microbiology* **12**

Firczuk M, Mucha A, Bochtler M (2005) **Crystal structures of active LytM** *Journal of Molecular Biology* **354**:578–590

Glauner B (1988) **Separation and quantification of muropeptides with high-performance liquid chromatography** *Analytical Biochemistry* **172**:451–464

Goedhart J (2021) **SuperPlotsOfData – a web app for the transparent display and quantitative comparison of continuous data from different conditions** *Molecular Biology of the Cell* **32**:470–474

Goley ED, Comolli LR, Fero KE, Shapiro Downing KH (2010) **DipM links peptidoglycan remodelling to outer membrane organization in Caulobacter** *Molecular Microbiology* **77**:56–73

Grabowska M, Jagielska E, Czapinska H, Bochtler M, Sabala I (2015) **High resolution structure of an M23 peptidase with a substrate analogue** *Scientific Reports* **5**

Serrano CK Gurnani, Winkle M, Martorana AM, Biboy J, More N, Moynihan P, Banzhaf M, Vollmer W, Polissi A (2021) **ActS activates peptidoglycan amidases during outer membrane stress in Escherichia coli** *Molecular Microbiology* **116**:329–342

Hallgren J, Tsirigos KD, Pedersen MD, Almagro Armenteros JJ, Marcatili P, Nielsen H, Krogh A, Winther O. (2022) **DeepTMHMM predicts alpha and beta transmembrane proteins using deep neural networks** *bioRxiv* https://doi.org/10.1101/2022.04.08.487609

Hartmann R, van Teeseling MCF, Thanbichler M, Drescher K. (2020) **BacStalk: A comprehensive and interactive image analysis software tool for bacterial cell biology** *Molecular Microbiology* **114**:140–150

Hay NA, Tipper DJ, Gygi D, Hughes C (1999) **A novel membrane protein influencing cell shape and multi-cellular swarming of Proteus mirabilis** *Journal of Bacteriology* **181**:2008–2016

Hughes HV, Lisher JP, Hardy GG, Kysela DT, Arnold RJ, Giedroc DP, Brun YV (2013) **Co-ordinate synthesis and protein localization in a bacterial organelle by the action of a penicillin-binding-protein** *Molecular Microbiology* **90**:1162–1177

Hussain S *et al.* (2018) **MreB filaments align along greatest principal membrane curvature to orient cell wall synthesis** *Elife* **7**

Jackson KM, Schwartz C, Wachter J, Rosa PA, Stewart PE (2018) **A widely conserved bacterial cytoskeletal component influences unique helical shape and motility of the spirochete Leptospira biflexa** *Molecular Microbiology* **108**:77–89

Jaqaman K, Loerke D, Mettlen M, Kuwata H, Grinstein S, Schmid SL, Danuser G (2008) **Robust single-particle tracking in live-cell time-lapse sequences** *Nature Methods* **5**:695–702

Jumper J *et al.* (2021) **Highly accurate protein structure prediction with AlphaFold** *Nature* **596**:583–589

Jung A, Eisheuer S, Cserti E, Leicht O, Strobel W, Möll A, Schlimpert S, Kühn J, Thanbichler M (2015) **Molecular toolbox for genetic manipulation of the stalked budding bacterium Hyphomonas neptunium** *Applied and Environmental Microbiology* **81**:736–744

Jung A, Rassbach A, Pulpetta RL, van Teeseling MCF, Heinrich K, Sobetzko P, Serrania J, Becker A, Thanbichler M. (2019) **Two-step chromosome segregation in the stalked budding bacterium Hyphomonas neptunium** *Nature Communications* **10**

Klein EA, Schlimpert S, Hughes V, Brun YV, Thanbichler M, Gitai Z (2013) **Physiological role of stalk lengthening in Caulobacter crescentus** *Communicative & Integrative Biology* **6**

Koch MK, McHugh CA, Hoiczyk E (2011) **BacM, an N-terminally processed bactofilin of Myxococcus xanthus, is crucial for proper cell shape** *Molecular Microbiology* **80**:1031–1051

Kühn J, Briegel A, Mörschel E, Kahnt J, Leser K, Wick S, Jensen GJ, Thanbichler M (2010) **Bactofilins, a ubiquitous class of cytoskeletal proteins mediating polar localization of a cell wall synthase in Caulobacter crescentus** *EMBO Journal* **29**:327–339

Kuru E, Tekkam S, Hall E, Brun YV, Van Nieuwenhze MS. (2015) **Synthesis of fluorescent D-amino acids and their use for probing peptidoglycan synthesis and bacterial growth in situ** *Nature Protocols* **10**:33–52

Kysela DT, Randich AM, Caccamo PD, Brun YV (2016) **Diversity takes shape: understanding the mechanistic and adaptive basis of bacterial morphology** *PLoS Biology* **14**

Larson MH, Gilbert LA, Wang X, Lim WA, Weissman JS, Qi LS (2013) **CRISPR interference (CRISPRi) for sequence-specific control of gene expression** *Nature Protocols* **8**:2180–2196

Leicht O, van Teeseling MCF, Panis G, Reif C, Wendt H, Viollier PH, Thanbichler M. (2020) **Integrative and quantitative view of the CtrA regulatory network in a stalked budding bacterium** *PLoS Genetics* **16**

Leifson E (1964) **Hyphomicrobium neptunium sp. n. Antonie Van Leeuwenhoek** :249–256

Letunic I, Bork P (2021) **Interactive Tree Of Life (iTOL) v5: an online tool for phylogenetic tree display and annotation** *Nucleic Acids Research* **49**:W293–W296

Lin L, Osorio Valeriano M, Harms A, Søgaard-Andersen L, Thanbichler M (2017) **Bactofilin-mediated organization of the ParABS chromosome segregation system in Myxococcus xanthus** *Nature Communications* **8**

Lord SJ, Velle KB, Mullins RD, Fritz-Laylin LK (2020) **SuperPlots: Communicating reproducibility and variability in cell biology** *Journal of Cell Biology* **219**

Lupas A (1996) **Prediction and analysis of coiled-coil structures** *Methods in Enzymology* **266**:513–525

Marblestone JG, Edavettal SC, Lim Y, Lim P, Zuo X, Butt TR (2006) **Comparison of SUMO fusion technology with traditional gene fusion systems: enhanced expression and solubility with SUMO** *Protein Science* **15**:182–189

Margolin W (2009) **Sculpting the bacterial cell** *Current Biology* **19**:R812–R822

Martinez LE, Hardcastle JM, Wang J, Pincus Z, Tsang J, Hoover TR, Bansil R, Salama NR (2016) **Helicobacter pylori strains vary cell shape and flagellum number to maintain robust motility in viscous environments** *Molecular Microbiology* **99**:88–110

McQuillen R, Xiao J (2020) **Insights into the structure, function, and dynamics of the bacterial cytokinetic FtsZ-ring** *Annual Review of Biophysics* **49**:309–341

Mistry J *et al.* (2021) **Pfam: The protein families database in 2021** *Nucleic Acids Research* **49**:D412–D419

Molisch H. (1907) **Die Purpurbakterien nach neuen Untersuchungen**

Möll A, Schlimpert S, Briegel A, Jensen GJ, Thanbichler M (2010) **DipM, a new factor required for peptidoglycan remodelling during cell division in Caulobacter crescentus** *Molecular Microbiology* **77**:90–107

Moore RL (1981) **The biology of Hyphomicrobium and other prosthecate, budding bacteria** *Annual Review of Microbiology* **35**:567–594

Munk AC *et al.* (2011) **Complete genome sequence of Rhodospirillum rubrum type strain (S1)** *Standards in Genomic Sciences* **4**:293–302

Nagai T, Ibata K, Es Park, Kubota M, Mikoshiba K, Miyawaki A (2002) **A variant of yellow fluorescent protein with fast and efficient maturation for cell-biological applications** *Nature Biotechnology* **20**:87–90

Oviedo-Bocanegra LM, Hinrichs R, Rotter DAO, Dersch S, Graumann PL (2021) **Single molecule/particle tracking analysis program SMTracker 2.0 reveals different dynamics of proteins within the RNA degradosome complex in Bacillus subtilis** *Nucleic Acids Research* **49**

Paysan-Lafosse T *et al.* (2022) **InterPro in 2022** *Nucleic Acids Research* **51**:D418–D427

Persat A, Stone HA, Gitai Z (2014) **The curved shape of Caulobacter crescentus enhances surface colonization in flow** *Nature Communications* **5**

Pfennig N, Trüper HG (1971) **Type and neotype strains of the species of phototrophic bacteria maintained in pure culture** *International Journal of Systematic Bacteriology* **21**:19–24

Plank M, Wadhams GH, Leake MC (2009) **Millisecond timescale slimfield imaging and automated quantification of single fluorescent protein molecules for use in probing complex biological processes** *Integrative Biology (Camb* **1**:602–612

Poggio S, Takacs CN, Vollmer W, Jacobs-Wagner C (2010) **A protein critical for cell constriction in the Gram-negative bacterium Caulobacter crescentus localizes at the division site through its peptidoglycan-binding LysM domains** *Molecular Microbiology* **77**:74–89

Postma M, Goedhart J (2019) **PlotsOfData—A web app for visualizing data together with their summaries** *PLOS Biology* **17**

R Development Core Team **R: a language and environment for statistical computing. The R Foundation for Statistical Computing**

Randich AM, Brun YV (2015) **Molecular mechanisms for the evolution of bacterial morphologies and growth modes** *Frontiers in Microbiology* **6**

Rohs PDA, Bernhardt TG (2021) **Growth and division of the peptidoglycan matrix** *Annual Review of Microbiology* **75**:315–336

Schindelin J *et al.* (2012) **Nature Methods** :676–682

Schneider CA, Rasband WS, Eliceiri KW (2012) **NIH Image to ImageJ: 25 years of image analysis** *Nature Methods* **9**:671–675

Shaner NC, Campbell RE, Steinbach PA, Giepmans BN, Palmer AE, Tsien RY (2004) **Improved monomeric red, orange and yellow fluorescent proteins derived from Discosoma sp. red fluorescent protein** *Nature Biotechnology* **22**:1567–1572

Shaner NC *et al.* (2013) **A bright monomeric green fluorescent protein derived from Branchiostoma lanceolatum** *Nature Methods* **10**:407–409

Shi C, Fricke P, Lin L, Chevelkov V, Wegstroth M, Giller K, Becker S, Thanbichler M, Lange A (2015) **Atomic-resolution structure of cytoskeletal bactofilin by solid-state NMR** *Science Advances* **1**

Shi H, Bratton BP, Gitai Z, Huang KC (2018) **How to Build a bacterial cell: MreB as the foreman of E. coli construction** *Cell* **172**:1294–1305

Sichel SR, Bratton BP, Salama NR (2022) **Distinct regions of H. pylori's bactofilin CcmA regulate protein-protein interactions to control helical cell shape** *Elife* **11**

Sycuro LK, Pincus Z, Gutierrez KD, Biboy J, Stern CA, Vollmer W, Salama NR (2010) **Peptidoglycan crosslinking relaxation promotes Helicobacter pylori's helical shape and stomach colonization** *Cell* **141**:822–833

Taylor JA *et al.* (2020) **Distinct cytoskeletal proteins define zones of enhanced cell wall synthesis in Helicobacter pylori** *Elife* **9**

Taylor JA, Sichel SR, Salama NR (2019) **Bent bacteria: A comparison of cell shape mechanisms in proteobacteria** *Annual Review of Microbiology* **73**:457–480

Thanbichler M, Shapiro L (2006) **MipZ, a spatial regulator coordinating chromosome segregation with cell division in Caulobacter** *Cell* **126**:147–162

Typas A, Banzhaf M, Gross CA, Vollmer W (2012) **From the regulation of peptidoglycan synthesis to bacterial growth and morphology** *Nature Reviews Microbiology* **10**:123–136

Uehara T, Parzych KR, Dinh T, Bernhardt TG (2010) **Daughter cell separation is controlled by cytokinetic ring-activated cell wall hydrolysis** *EMBO Journal* **29**:1412–1422

van den Ent F, Johnson CM, Persons L, de Boer P, Löwe J. (2010) **Bacterial actin MreB assembles in complex with cell shape protein RodZ** *EMBO Journal* **29**:1081–1090

van Niel CB. (1944) **The culture, general physiology, morphology, and classification of the non-sulfur purple and brown bacteria** *Bacteriological Reviews* **8**:1–118

van Teeseling MCF, de Pedro MA, Cava F. (2017) **Determinants of bacterial morphology: from fundamentals to possibilities for antimicrobial targeting** *Frontiers in Microbiology* **8**

Varadi M *et al.* (2022) **AlphaFold Protein Structure Database: massively expanding the structural coverage of protein-sequence space with high-accuracy models** *Nucleic Acids Research* **50**:D439–D444

Vasa S, Lin L, Shi C, Habenstein B, Riedel D, Kühn J, Thanbichler M, Lange A (2015) **β-Helical architecture of cytoskeletal bactofilin filaments revealed by solid-state NMR** *Proceedings of the National Academy of Sciences U S A* **112**:E127–136

Vollmer W, Blanot D, de Pedro MA. (2008) **Peptidoglycan structure and architecture** *FEMS Microbiology Reviews* **32**:149–167

Wagner JK, Brun YV (2007) **Out on a limb: how the Caulobacter stalk can boost the study of bacterial cell shape** *Molecular Microbiology* **64**:28–33

Wali TM, Hudson GR, Danald DA, Weiner RM (1980) **Timing of swarmer cell cycle morphogenesis and macromolecular synthesis by Hyphomicrobium neptunium in synchronous culture** *Journal of Bacteriology* **144**:406–412

Wong F, Garner EC, Amir A (2019) **Mechanics and dynamics of translocating MreB filaments on curved membranes** *Elife* **8**

Yang DC, Blair KM, Salama NR (2016) **Staying in shape: the impact of cell shape on bacterial survival in diverse environments** *Microbiology and Molecular Biology Reviews* **80**:187–203

Zuckerman DM, Boucher LE, Xie K, Engelhardt H, Bosch J, Hoiczyk E (2015) **The bactofilin cytoskeleton protein BacM of Myxococcus xanthus forms an extended beta-sheet structure likely mediated by hydrophobic interactions** *PLoS One* **10**

Article and author information

Sebastian Pöhl
Department of Biology, University of Marburg, Marburg, Germany

Manuel Osorio-Valeriano
Department of Biology, University of Marburg, Marburg, Germany, Max Planck Institute for Terrestrial Microbiology, Marburg, Germany

Emöke Cserti
Department of Biology, University of Marburg, Marburg, Germany

Jannik Harberding
Department of Biology, University of Marburg, Marburg, Germany

Rogelio Hernández-Tamayo
Max Planck Institute for Terrestrial Microbiology, Marburg, Germany, Department of Chemistry, University of Marburg, Marburg, Germany, Center for Synthetic Microbiology (SYNMIKRO), Marburg, Germany

Jacob Biboy
Centre for Bacterial Cell Biology, Biosciences Institute, Newcastle University, Newcastle upon Tyne, United Kingdom
ORCID iD: 0000-0002-1286-6851

Patrick Sobetzko
Center for Synthetic Microbiology (SYNMIKRO), Marburg, Germany

Waldemar Vollmer
Centre for Bacterial Cell Biology, Biosciences Institute, Newcastle University, Newcastle upon Tyne, United Kingdom, Institute for Molecular Bioscience, The University of Queensland, Brisbane, Australia
ORCID iD: 0000-0003-0408-8567

Peter L. Graumann
Department of Chemistry, University of Marburg, Marburg, Germany, Center for Synthetic Microbiology (SYNMIKRO), Marburg, Germany

Martin Thanbichler
Department of Biology, University of Marburg, Marburg, Germany, Max Planck Institute for Terrestrial Microbiology, Marburg, Germany, Center for Synthetic Microbiology (SYNMIKRO), Marburg, Germany
For correspondence: thanbichler@uni-marburg.de
ORCID iD: 0000-0002-1303-1442

Copyright

Editors

Reviewing Editor
Sonja Albers
University of Freiburg, Freiburg, Germany

Senior Editor
Dominique Soldati-Favre
University of Geneva, Geneva, Switzerland

Reviewer #1 (Public Review):

In their study, Osorio-Valeriano and colleagues seek to understand how bacterial-specific polymerizing proteins called bactofilins contribute to morphogenesis. They do this primarily in the stalked budding bacterium Hyphomonas neptunium, with supporting work in a spiral-shaped bacterium, Rhodospirillum rubrum. Overall the study incorporates bacterial genetics and physiology, imaging, and biochemistry to explore the function of bactofilins and cell wall hydrolases that are frequently encoded together within an operon. They demonstrate an important, but not essential, function for BacA in morphogenesis of H. neptunium. Using biochemistry and imaging, they show that BacA can polymerize and that its localization in cells is dynamic and cell-cycle regulated. They further demonstrate that BacA likely limits movement of the elongasome into the stalk, spatially confining its activity. The authors then focus on lmdC, which encodes a putative M23 endopeptidase upstream of bacA in H. neptunium, and find that is essential for viability. The purified LmdC C-terminal domain could cleave E. coli peptidoglycan in vitro suggesting that it is a DD-endopeptidase. LmdC interacts directly with BacA in vitro and co-localizes with BacA in cells. To expand their observations, the authors then explore a related endopeptidase/bactofilin pair in R. rubrum; those observations support a function for LmdC and BacA in R. rubrum morphogenesis as well.

An overall strength of this study is the breadth and completeness of approaches used to assess bactofilin and endopeptidase function in cells and in vitro. The authors establish a clear function for BacA in morphogenesis in two bacterial systems, and demonstrate a physical relationship between BacA and the cell wall hydrolase LmdC that may be broadly conserved. The eventual model the authors favor for BacA regulation of morphogenesis in H. neptunium is that it serves as a diffusion barrier and limits movement of morphogenetic machinery like the elongasome into the elongating stalk and/or bud.

The data presented illuminate aspects of bacterial morphogenesis and the physical and functional relationship between polymerizing proteins and cell wall enzymes in bacteria, a recurring theme in bacterial cell biology with a variety of underlying mechanisms. Bactofilins in particular are relatively recently discovered and any new insights into their functions and mechanisms of action are valuable. The findings presented here are likely to interest those studying bacterial morphogenesis, peptidoglycan, and cytoskeletal function.

- https://doi.org/10.7554/eLife.86577.2.sa1

Reviewer #2 (Public Review):

This is an excellent study. It starts with the identification of two bactofilins in H. neptunium, a demonstration of their important role for the determination of cell shape and discovery of an associated endopeptidase to provide a convincing model for how these two classes of proteins interact to control cell shape. This model is backed up by a quantitative characterisation of their properties using high-resolution imaging and image analysis methods.

Overall, all evidence is very convincing and I do not have many recommendations on how to improve the manuscript.

In my opinion, there are only two issues that I have with the paper:

1. The single particle dynamics of BacA is presented and analysed and I would like to give some suggestions on how to maybe extract even more information from the already acquired data:

1.1. Presentation: Figure 5A is only showing projections of single particle time-lapse movies. To convince the reader that it was indeed possible to detect single molecules it would be helpful if the authors present individual snapshots and intensity traces. In case of single molecules these will show step wise bleaching
1.2. Analysis: Figure 5B and Supplement Figure 1 are showing the single particle tracking results, revealing that there are two populations of BacA-YFP in the cell. However, this data does not show if individual BacA particles transition between these two populations or not. A more detailed analysis of the existing data, where one can try to identify confinement events in single particle trajectories could be very revealing and help to understand the behaviour of BacA in more detail.

2. The title of Fig. 3 says that BacA and BacD copolymerise, however, the data presented to confirm this conclusions is actually rather weak. First, the Alphafold prediction does not show the co-polymer, and second, the in vitro polymerisation experiments were only done with BacA in the absence of BacD. Accordingly, the only evidence that supports this is their colocalization in fluorescence microscopy. I suggest to either weaken the statement or change the title and add more evidence.

Finally, did the authors think about biochemical experiments to study the interaction between the cytoplasmic part of LmdC and the bactofilins? These could further support their model.

- https://doi.org/10.7554/eLife.86577.2.sa0

Author Response

The following is the authors' response to the original reviews.

We thank the two reviewers for their constructive criticism, which helped to significantly improve our manuscript.

During the revision process, we had to realize that the localization pattern reported for H. neptunium LmdCN-mCherry was an artifact caused by bleed-through of the BacA-YFP signal in the mCherry channel. More detailed studies showed that the fusion protein was detectable by Western blot analysis but, for unknown reasons, did not produce any fluorescence signal. Therefore, we have now removed the localization data shown in previous Figure 8B,C and Figure 8—figure supplement 1.

To provide more evidence for a functional interaction between BacA and LmdC in H. neptunium, we have now established an inducible CRISPR interference system for this species and used it successfully to deplete LmdC (new Figure 9A-F). The loss of LmdC causes morphological defects very similar to those observed for the ΔbacA(D) mutant. In line with the physical interaction of BacA with the cytoplasmic region of LmdC observed in vitro, these findings support the hypothesis that the two proteins act in the same pathway. Consistent with the results obtained in H. neptunium, the absence of BacA leads to the delocalization of LmdC in R. rubrum. Moreover, we now provide in vivo evidence for a critical role of the cytoplasmic region of LmdC in the interaction of this protein with BacA in R. rubrum cells (new Figure 11). Together, these new findings strongly support the model that BacA and LmdC form a conserved morphogenetic module involved in the establishment of complex cell shapes in bacteria.

Please see below for a more detailed explanation of our new results and for our response to the issues raised in the first round of review.

Response to reviewers

We thank the two reviewers for their constructive criticism, which helped to significantly improve our manuscript.

During the revision process, we had to realize that the localization pattern reported for H. neptunium LmdCN-mCherry was an artifact caused by bleed-through of the BacA-YFP signal in the mCherry channel. More detailed studies showed that the fusion protein was detectable by Western blot analysis but, for unknown reasons, did not produce any fluorescence signal. Therefore, we have now removed the localization data shown in previous Figure 8B,C and Figure 8—figure supplement 1.

To provide more evidence for a functional interaction between BacA and LmdC in H. neptunium, we have now established an inducible CRISPR interference system for this species and used it successfully to deplete LmdC (new Figure 9A-F). The loss of LmdC causes morphological defects very similar to those observed for the ΔbacA(D) mutant. In line with the physical interaction of BacA with the cytoplasmic region of LmdC observed in vitro, these findings support the hypothesis that the two proteins act in the same pathway. Consistent with the results obtained in H. neptunium, the absence of BacA leads to the delocalization of LmdC in R. rubrum. Moreover, we now provide in vivo evidence for a critical role of the cytoplasmic region of LmdC in the interaction of this protein with BacA in R. rubrum cells (new Figure 11). Together, these new findings strongly support the model that BacA and LmdC form a conserved morphogenetic module involved in the establishment of complex cell shapes in bacteria.

Please see below for a more detailed explanation of our new results and for our response to the issues raised in the first round of review.

Reviewer #1 (Public Review)

In their study, Osorio-Valeriano and colleagues seek to understand how bacterial-specific polymerizing proteins called bactofilins contribute to morphogenesis. They do this primarily in the stalked budding bacterium Hyphomonas neptunium, with supporting work in a spiral-shaped bacterium, Rhodospirillum rubrum. Overall the study incorporates bacterial genetics and physiology, imaging, and biochemistry to explore the function of bactofilins and cell wall hydrolases that are frequently encoded together within an operon. They demonstrate an important, but not essential, function for BacA in morphogenesis of H. neptunium. Using biochemistry and imaging, they show that BacA can polymerize and that its localization in cells is dynamic and cell-cycle regulated. The authors then focus on lmdC, which encodes a putative M23 endopeptidase upstream of bacA in H. neptunium, and find that is essential for viability. The purified LmdC C-terminal domain could cleave E. coli peptidoglycan in vitro suggesting that it is a DD-endopeptidase. LmdC interacts directly with BacA in vitro and co-localizes with BacA in cells. To expand their observations, the authors then explore a related endopeptidase/bactofilin pair in R. rubrum; those observations support a function for LmdC and BacA in R. rubrum morphogenesis as well.

An overall strength of this study is the breadth and completeness of approaches used to assess bactofilin and endopeptidase function in cells and in vitro. The authors establish a clear function for BacA in morphogenesis in two bacterial systems, and demonstrate a physical relationship between BacA and the cell wall hydrolase LmdC that may be broadly conserved. The eventual model the authors favor for BacA regulation of morphogenesis in H. neptunium is that it serves as a diffusion barrier and limits movement of morphogenetic machinery like the elongasome into the elongating stalk

> *and/or bud. However, there is no data presented here to address that model and the role of LmdC in H. neptunium morphogenesis remains unclear.*

We hypothesize that BacA establishes a barrier that prevents the movement of elongasome complexes into the stalk, either directly by sterical hindrance and/or indirectly by promoting the formation of an annular region of high positive inner cell curvature that cannot be passed by the elongasome. To test this model, we have now analyzed the localization dynamics of RodZ, a core structural component of the elongasome complex, in wild-type and ΔbacAD cells. We found that wild-type cells show dynamic YFP-RodZ foci whose movement is limited to the mother cell and the nascent bud, with no signal ob-served in the stalk. In ΔbacAD cells, by contrast, the fusion protein is consistently detected in all regions of the cell, including nascent stalks (new Figure 5). These results support the idea that BacA is required to confine the elongasome to the mother cell and bud regions and, thus, set the limits of the different growth zones in H. neptunium. We also attempted to follow the localization dynamics of other elongasome components, such as PBP2, MreC and MreD, but none of the corresponding fluorescent protein fusions was functional.

In the past, we tried intensively to generate conditional mutants of lmdC, but all attempts to place the expression of this gene under the control of the copper- or zinc-inducible promoters available for H. neptunium were unsuccessful. To clarify the role of LmdC in H. neptunium morphogenesis, we have now established an inducible CRISPR interference system for this species and managed to block the ex-pression of lmdC using an sgRNA directed against the 5' region of its non-coding strand. We observed that cells lacking LmdC show a phenotype very similar to that of the ΔbacA mutant. Together with the finding that the N-terminal cytoplasmic region of LmdC physically interacts with BacA, this result strongly supports the hypothesis that BacA and LmdC act in the same pathway, forming a complex that ensures proper morphogenesis in H. neptunium (new Figure 9).

> *The data presented illuminate aspects of bacterial morphogenesis and the physical and functional relationship between polymerizing proteins and cell wall enzymes in bacteria, a recurring theme in bacterial cell biology with a variety of underlying mechanisms. Bactofilins in particular are relatively recently discovered and any new insights into their functions and mechanisms of action are valuable. The findings presented here are likely to interest those studying bacterial morphogenesis, peptido-glycan, and cytoskeletal function.*
>
> ***Reviewer #2 (Public Review):***
>
> *This is an excellent study. It starts with the identification of two bactofilins in H. neptunium, a demonstration of their important role for the determination of cell shape and discovery of an associated endopeptidase to provide a convincing model for how these two classes of proteins interact to control cell shape. This model is backed up by a quantitative characterisation of their properties using high-resolution imaging and image analysis methods.*
>
> *Overall, all evidence is very convincing and I do not have many recommendations on how to improve the manuscript.*
>
> *In my opinion, there are only two issues that I have with the paper:*
>
> 1. *The single particle dynamics of BacA is presented as analysed and I would like to give some suggestions how to maybe extract even more information from the already acquired data:*
>
> *1.1. Presentation: Figure 5A is only showing projections of single particle time-lapse movies. To convince the reader that it was indeed possible to detect single molecules it*

> *would be helpful if the authors present individual snapshots and intensity traces. In case of single molecules these will show step wise bleaching.*

We have now added a supplementary video that shows both time series and intensity traces of individual BacA-YFP molecules (Figure 6—Video 1). It verifies the step-wise bleaching of the particles observed and thus shows that we observe the mobility of single molecules. Moreover, we have now included a supplementary figure that shows all trajectories identified within representative cells. This visualization provides a more comprehensive view of our data and further supports the notion that our analysis is based on the detection of single molecules.

> *1.2. Analysis: Figure 5B and Supplement Figure 1 are showing the single particle tracking results, revealing that there are two populations of BacA-YFP in the cell. However, this data does not show if individual BacA particles transition between these two populations or not. A more detailed analysis of the existing data, where one can try to identify confinement events in single particle trajectories could be very revealing and help to understand the behaviour of BacA in more detail.*

We agree that an analysis of the single-molecule traces for transitions between the mobile and static states would help to achieve a more detailed understanding of the polymerization behavior of BacA. We believe that the dynamic formation, reorganization and disappearance of BacA-YFP foci observed by time-lapse analysis (Figure 4) indicates that BacA undergoes reversible polymerization in vivo. A deeper investigation of this aspect is beyond the scope of the present study and will be performed at a later point.

> *1. The title of Fig. 3 says that BacA and BacD copolymerise, however, the data presented to confirm this conclusion is actually rather weak. First, the Alphafold prediction does not show the co-polymer, and second, the in vitro polymerisation experiments were only done with BacA in the absence of BacD. Accordingly, the only evidence that supports this is their colocalization in fluorescence microscopy. I suggest either weakening the statement or changing the title adds more evidence.*

To support the idea that BacA and BacD interact with each other, we have now added images of cells producing BacA-YFP or BacD-CFP individually (new Figure 3—figure supplement 1B,C). The results obtained show that Bac-YFP alone still forms filamentous structures, whereas BacD-CFP condenses into tight foci in the absence of its paralog. However, when produced together with BacA-YFP, the two proteins colocalize into filamentous structures, supporting the notion that they interact with each other. However, we agree that it is unclear whether BacA and BacD copolymerize into mixed protofilaments or whether they form distinct protofilaments that then interact laterally to form larger bundles. We have therefore replaced the term “co-polymerize” with “assemble” in the heading of this section.

> *Finally, did the authors think about biochemical experiments to study the interaction between the cytoplasmic part of LmdC and the bactofilins? These could further support their model.*

We show the interaction between the cytoplasmic region of H. neptunium LmdC and BacA in Figure 9G,H (previously Figure 8D,E). For technical reasons, it was not possible to synthesize a peptide com-prising the corresponding region of R. rubrum LmdC, so that our in vitro analysis is limited to the H. neptunium proteins.

> *To further support the notion that BacA interacts with the cytoplasmic region of LmdC, we have now analyzed the localization behavior of two LmdC variants with amino acid exchanges in the conserved cytoplasmic β-hairpin motif (new Figure 11). Both variants no*

> *longer colocalize with BacA and are no longer enriched at the inner cell curve. Interestingly, these exchanges also affect the enrichment of BacA at the inner cell curvature, suggesting that BacA needs to interact with LmdC for proper localization. It is tempting to speculate that BacA polymers have a preferred intrinsic curvature and that the activity of the BacA-LmdC complexes adjusts cell curvature in a manner that facilitates their association with the inner curve.*
>
> ***Reviewer #1 (Recommendations for The Authors):***
>
> *We have the following specific recommendations for the improvement of the manuscript:*

1. *Several places would benefit from additional quantitation of data:*

> *a. Figure 1 and supplements: can cell shape be quantified in a more specific way? (e.g. principle component analysis of shape as in https://onlinelibrary.wiley.com/doi/10.1111/mmi.13218). It looks as if BacD production may partially rescue the bacA shape phenotype?*

We have made considerable efforts to establish methods to quantify morphological changes and protein localization patterns in Hyphomonas neptunium. Since standard software packages, such as Oufti or MicrobeJ, are not able to reliably detect stalks and, thus, typically identify buds as separate cells, we have developed our own analysis software (BacStalk; Hartmann et al, 2020, Mol Microbiol), that is optimized for the detection of thin cellular extensions. However, while this software works very well with wild-type cells, it also fails to recognize amorphous cells with multiple, ill-defined extensions. Given these problems in cell segmentation, it is currently not possible to use principle component analysis to obtain a robust measure of the morphological defects of bactofilin mutants in H. neptunium.

> *b. Figures 2-S2b, 7D and 9-S1b - can the area under the peaks be quantified and compared across strains? Visual examination of the spectra makes it difficult to discern differences.*

A direct comparison of the peak areas between strains is not possible, because the absolute values depend on the amount of peptidoglycan used in the muropeptide analyses. It is very difficult to precisely quantify peptidoglycan, which makes it challenging to use equal amounts of material from different strains in the reactions. However, the relative proportion of different muropeptide species, as provided in Figure 2—Dataset 1, faithfully reflects the composition of peptidoglycan and can easily compared between strains.

> *c. Figure 9E,F, 9-S4d - BacA and LmdC localization in R. rubrum is very difficult to assess. It does not look linear/filamentous in most cells and is difficult to tell if it is associated with the inner curvature. Can you quantify the position of the signal along the short axis of the cell to better demonstrate that?*

We agree that a better quantification of the distribution of protein along the cell envelope of R. rubrum is required to support the conclusions drawn. To address this issue, we have now used line scans to measure the fluorescence intensities along the inner and outer curve of cells (n=200 per strain) and visualized the data in the form of demographs. The results clearly show an enrichment of BacA and LmdC at the inner curve in wild-type cells and a disruption of this pattern in various mutant backgrounds (new Figures 10F,G,J and 11D,E).

> 1. *Figure 2-S2A. Does ΔbacD grow better than wild-type? It would also be useful to add growth curves of the bacA complemented strains.*

In the case of H. neptunium growth curves are often misleading, because cells start to aggregate at the late exponential phase due to abundant EPS formation. The degree of cell aggregation also depends on the morphology of cells, because EPS production is limited to the mother cell body, which makes it challenging to compare morphologically distinct mutant strains. We have now performed growth assays for all H. neptunium deletion and complementation strains used in the study and limited the analysis of doubling times to the early and mid-exponential phase, in which cells do not yet form visible aggregates. The results obtained are now included in the new Figure 1F and Figure 1—figure supplement 2D. They show that the doubling times of the different bactofilin mutants are close to that of the wild-type strain.

> 1. *Figure 4BC: From the demographs provided, BacA and BacD appear to have different localization dynamics. BacD seems to stay at the base of the stalk, nearest the mother cell, whereas BacA migrates towards to bud? Also, "length" is misspelt in the panels.*

During the transition to bud formation, we indeed observe that the localization patterns of BacA and BacD are in many cases not fully superimposable, with BacD lagging behind BacA and forming transient additional clusters in the vicinity of the stalk base. Examples are now shown in Figure 4—figure supplement 4). This effect explains the distinct patterns in the demographs. We have now modified the text accordingly. We have also corrected the spelling of “length” in the figure.

> 1. *Can BacD polymerize on its own? It colocalizes with BacA in E. coli but that does not necessarily mean it co-polymerizes.*

Please see our response to a similar issue (point 2) raised by Reviewer #1.

> 1. *Lines 263-266. You use E. coli PG as a substrate for LmdC in vitro because "peptidoglycan from H. neptunium shows only a low degree of cross-linkage and hardly any pentapeptides." Does this not have relevance to the physiological significance of the observed activity? Or do you presume that LmdC activity (and/or that of other endopeptidases) is very high in H. neptunium so it is difficult to detect additional activity using HnPG as a substrate? It would be useful to clarify this logic in the text.*

DD-crosslinks are formed by all major peptidoglycan biosynthetic complexes, including the elongasome and the divisome, so that their general relevance to cell growth in H. neptunium is beyond doubt. The low degree of crosslinkage observed suggests that H. neptunium contains high endopeptidase activity, which cleaves crosslinks after their formation by DD-transpeptidases. We have now added the explanation “likely due to a high level of autolytic activity” to make this point clearer. Whether LmdC makes a major contribution to the low level of crosslinkage remains to be determined. However, our data suggest that it mostly acts in complex with BacA, so that it may only cleave peptidoglycan locally and not have a global effect global on cell wall composition. It would not possible to detect the DD-endopeptidase activity of LmdC using H. neptunium peptidoglycan as a substrate, because it has a low content of DD-linked peptide chains. To facilitate the in vitro activity assay, we therefore used highly crosslinked peptidoglycan from a mutant E. coli strain.

> 1. *Lines 268-269: Is there some explanation for why monomers do not increase on LmdC treatment? Here quantitation of peaks before and after treatment would allow the reader to more precisely interpret these data.*

The absolute peak sizes are not comparable, because there is some variation in the amount of peptido-glycan included in the assays (see also our comments on point 1b raised by Reviewer #1) and the integrated peak areas (which correspond to the amounts of muropeptide species produced) depend on both the height and the width of the peaks, which vary to some degree in different HPLC runs. The relevant measure to compare the muropeptide profiles is therefore the relative content of different muropeptide species in the different conditions. For clarification, we have now added the following sentence to the legend of Figure 8D: “A quantification of the relative abundance of different muropeptide species in each condition, based on a comparison of the relative integrated peak areas, is provided in Figure 8—Dataset 1.” The control reaction lacking LmdC only contains peptidoglycan diluted in buffer and thus provides insight into muropeptide composition of untreated peptidoglycan.

> 1. *Lines 280-283: It would be interesting to know if the transmembrane domain of LmdC is required for its localization since it is dispensable for binding BacA and since LmdC still localizes to foci without BacA.*

Given that it is currently not possible to localize LmdC in H. neptunium, we were not able to perform this analysis.

> 1. *Line 296: it is also possible that LmdC localizes with another protein and does not independently assemble into larger complexes.*

Since the localization pattern reported for LmdC in the ΔbacAD background is no longer valid, we have not discussed this aspect in the revised version of our manuscript. However, in general, we do not exclude the possibility that LmdC could interact with other peptidoglycan biosynthetic proteins.

> 1. *Line 304-306 and Fig 9: Is the domain organization of RrLmdC the same as for HnLmdC? It would be useful to include its domain organization as well. Also, please add amino acid numbering to Figure 9B.*

We have now added a schematic showing the domain organization of LmdC from R. rubrum (new Figure 10B). The protein is highly similar to its homolog from H. neptunium.

> 1. *Line 340-341: "In both cases, they functionally interact with LmdC-type DD-endopeptidases to promote local changes in the pattern of peptidoglycan biosynthesis." This conclusion is not experimentally supported. Since LmdC is essential and you could not make a depletion strain in H. neptunium, it was not shown that the interaction with LmdC is how BacA promotes changes in PG patterning. HADA/FDAA labeling was not performed in R. rubrum, and no global changes in PG chemistry were observed in bacA or lmdC mutants, so you cannot claim BacA or LmdC influences PG patterning there, either. Either soften this statement to a hypothesis or otherwise rephrase.*

To further corroborate a functional interaction between BacA and LmdC, we have now established an inducible CRISPRi system to deplete LmdC from H. neptunium cells (see also our comments on the public review of Reviewer #1). We observe that the loss of LmdC leads to a phenotype very similar to that observed for the ΔbacA(D) mutant, supporting the idea that BacA and LmdC act in the same path-way. We have now also performed localization studies of the elongasome component RodZ in H. nep-tunium, which demonstrate that the spatial distribution of elongasome complexes is affected in the absence of the bactofilin cytoskeleton in H. neptunium. Combined with the observation that LmdC is a catalytically active DD-endopeptidase and its absence leads to morphological defects, these results

indicate that BacA, together with LmdC, induces local changes in pattern of peptidoglycan biosynthesis, both by affecting elongasome movement and, likely, by reducing peptidoglycan crosslinking in the cell envelope regions it occupies.

> 1. *Figure 9-S4: there is no panel C (change D to C).*

Corrected.

> 1. *Lines 344-355: No data is presented here to support the barrier model of bactofilin function. In addition, it is unclear why cells would take on amorphous shapes instead of extended rod shapes/filaments if elongasome function was not constrained on the longitudinal axis. It would be helpful to have more discussion of the potential mechanisms of LmdC function in H. neptunium in this section of the discussion since that is the emphasis of the results section.*

To support the barrier model, we have now compared the localization dynamics of the elongasome component RodZ in wild-type and ΔbacAD cells. The results show that RodZ is excluded from the stalk in the wild-type background, whereas it readily enters the stalk in the mutant cells, leading to the expansion of stalks into large, amorphous extensions. Consistent with these findings, HADA labeling is not observed within the stalks in wild-type cells, whereas it is readily observed in the enlarged stalk structures (pseudohyphae) formed in the mutant cells.

The current model of MreB movement suggests that MreB filaments have an intrinsic curvature and thus preferentially align along regions of similar curvature, which is along the circumference of the cell in rod-shaped geometries. However, previous work has shown that MreB starts to move along randomly oriented trajectories as soon as cells lose their rod-shaped morphology and adopt more spherical shapes (Hussain et al, 2018, eLife). In line with these findings, our current and our previous work (Cserti et al, 2017, Mol Microbiol) indicate that the expansion of the ovoid H. neptunium mother cell prior to the onset of stalk biosynthesis as well as bud formation are mediated by the elongasome complex. Thus, the elongasome can clearly also give rise to shapes other than rods. Interestingly, however, the H. neptunium elongasome also appears to drive the formation of the rod-shaped stalk, possibly by moving around the circumference of the stalk base. Thus, species- or growth phase-dependent regulatory mechanisms or, potentially, differences in the spatial arrangement of the glycan strands within the peptido-glycan layer may result in different modes of elongasome movement and, thus, modulate the morphogenetic activity of elongasome complexes.

> 1. *Lines 395-397: It is also possible that LmdC positioning is dependent on cell morphology, rather than directly on BacA, since morphology is so distorted in bacA mutant cells.*

We provide several lines of evidence showing that LmdC and BacA functionally and physically interact (see above), making it highly unlikely that the two proteins are not associated with each other. How-ever, our previous (Figure 10I,J) and new (Figure 11) results suggest that the physical interaction with LmdC and/or or the cell shape-modulating activity of the complex are required for the proper localization of BacA at the inner curve of the cell. This finding may indicate the existence of a self-reinforcing cycle, in which the morphological changes induced by BacA-LmdC assemblies stimulate the recruitment of additional assemblies to their site of action.